NUMERICAL STUDY OF THREE VISCOUS / INVISCID INTERACTION METHODS

THESIS

Jeffrey C. Tromp

AFIT/GA/AA/88S-1

DEPARTMENT OF THE AIR FORCE
AIR UNIVERSITY
AIR FORCE INSTITUTE OF TECHNOLOGY

Wright-Patterson Air Force Base, Ohio

AFIT/GA/AA/88S-01

NUMERICAL STUDY OF THREE VISCOUS / INVISCID INTERACTION METHODS

THESIS

Jeffrey C. Tromp

AFIT/GA/AA/88S-1

AFIT/GA/AA/88S-1

NUMERICAL STUDY OF THREE VISCOUS / INVISCID INTERACTION METHODS

THESIS

Presented to the Faculty of the School of Engineering
of the Air Force Institute of Technology
Air University
In Partial Fulfillment of the
Requirements for the Degree of
Master of Science in Astronautical Engineering

Jeffrey C. Tromp

September 1988

Approved for public release; distribution unlimited

Preface

The efficient calculation of flows with viscous/inviscid interaction has been the topic of much research over the past several years. Three algorithms were developed to solve the viscous/inviscid problem. The first method uses finite difference equations with successive line over-relaxation (SLOR) sweeps for solving the approximate Navier-Stokes equations in the viscous region and the stream function equation in the inviscid region. An implicit coupling scheme is developed to match the two solutions. The second method uses finite difference approximations for solving the stream function equation in the inviscid region and a fourth order Runge-Kutta method for solving the integral boundary layer equations in the viscous region. In the third method, the inviscid flow solution is obtained by a panel method, while the viscous flow solution is obtained using the finite difference form for the boundary layer equations operating in an inverse scheme.

I would like to thank Dr. A. Halim for his extensive technical assistance with this work and for supervising this thesis, and Dr. Shang of the Flight Dynamics Laboratory for his encouragement and insightful comments. Special thanks goes to Lisa, my fiancee, for her understanding and support over the last year.

The ASD Cyber was used extensively as the computational resource of this study. I would like to acknowledge the Flight Control Division of the Flight Dynamics Laboratory, (AFWAL/FIG) for sponsoring the work performed on the Cyber and for allowing me the time away from my normal duties to conduct this research.

List of Figures

Table Of Contents

List of Symbols

a	finite difference coefficient
A	finite difference coefficient, constant
AU	velocity profile coefficient
α	inviscid transformation parameter
b	finite difference coefficient
B	finite difference coefficient, constant
BU	velocity profile coefficient
β	recurrence coefficient, and inviscid transformation parameter
C	finite difference coefficient, constant, constant of integration
CU	velocity profile coefficient
C_f	skin friction coefficient
CF	skin friction coefficient
d	finite difference coefficient, differential operator
dx	differential of x
D	finite difference coefficient, constant
DS	displacement thickness
DU	velocity profile coefficient
DUE	maximum difference in U_e
DUEMAX	DUE at first iteration
δ	boundary layer thickness
δu	viscous correction to inviscid velocity
δ^*	displacement thickness

$\Delta\eta$	grid size in normal direction
$\Delta\xi$	grid size in streamwise direction
E	finite difference coefficient, constant
EU	velocity profile coefficient
η	normal distance in computational domain
F	finite difference coefficient
FU	velocity profile coefficient
F_1	Function of C_f and δ
F_2	Function of C_f and δ
γ	recurrence coefficient
H	inviscid transformation scale factor
K	intermediate variable in IBL equations
L	characteristic length
M	intermediate variable in IBL equations
μ	viscosity
n	solution level
ν	kinematic viscosity
ω	vorticity
ω^*	wall vorticity at inlet boundary
p	pressure
P	finite difference coefficient, intermediate variable in IBL equations
PSI	stream function
PY	Howarth velocity profile function
Ψ	stream function
q	source strength

Q	finite difference coefficient, intermediate variable in IBL equations
r	distance from source to $\delta^*(x)$
R	recurrence coefficient, residual
RMAX	residual from first iteration
R_e	Reynolds number
RHS	right hand side of a finite difference equation
ρ	density
S	recurrence coefficient
SQREN	$R_e^{1/2}$
T	recurrence coefficient
τ_w	wall shear stress
θ	momentum thickness, source angle
u	streamwise velocity component
U_e	streamwise velocity at boundary layer edge
UE	streamwise velocity at boundary layer edge
UM	parameter that is zero when u>0, and equal to -u when u<0
UP	parameter that is zero when u<0, and equal to u when u>0
v	normal velocity component
V	total velocity
V_e	normal velocity at boundary layer edge
W	relaxation parameter
x	distance in streamwise direction
x_1	x position at inlet boundary

x_2	x position at downstream boundary
X_0	Howarth corner velocity position
ξ	streamwise distance in computational domain, dummy index of integration
y	distance in normal direction
Y	y times $R_e^{1/2}$
Y_1	Y at interface
Y_2	Y at outer boundary
z	intermediate variable in IBL equations
ζ	inviscid transformation parameter

Subscripts

bl	boundary layer
h	Hilbert
i	grid index for streamwise direction
j	grid index for normal direction
ξ	denotes derivative with respect to ξ
η	denotes derivative with respect to η
x	denotes derivative with respect to x
y	denotes derivative with respect to y
∞	free-stream condition

Abstract

The study of flows with viscous/inviscid interaction has attracted many researchers over the last decade. These flows occur whenever the adverse pressure gradient is large enough to cause flow separation. The current emphasis is to find efficient ways of solving these types of flows without solving the full Navier-Stokes equations.

Three methods for solving the viscous/inviscid problem were studied. The first method uses finite difference equations to model both the viscous and inviscid regions. A coupling scheme is developed to match the two solutions. The second method solves the integral boundary layer equations in the viscous region and finite difference equations in the inviscid region. The third method solves the Hilbert integral to generate a correction to the inviscid velocity using the boundary layer equations as the viscous model. The model problem used in this work is Howarth flow over a flat plate.

The three methods were evaluated in terms of solution accuracy, memory requirements, and computation times.

NUMERICAL STUDY OF THREE VISCOUS / INVISCID INTERACTION METHODS

I Introduction

The aerodynamic performance of a flight vehicle is greatly affected by the accuracy of the computational or experimental methods used in the design process. Any successful design must carefully account for the drag. The viscous calculations have a substantial impact on the drag estimation. Naturally, the full Navier-Stokes (NS) equations correctly estimate the drag on a flight vehicle. However, their use can be costly and in many cases unnecessary.

Recent research has focused on the use of alternative forms of the NS equations. These approximate sets of equations are simpler and require fewer computations than the NS equations, but are valid only as long as their simplifying assumptions are not violated. For example, high Reynolds number flows over a body usually result in the formation of a thin shear layer close to its surface. For this type of flow the pressure gradient normal to the body and viscous terms with derivatives in the streamwise direction can be neglected by an order of magnitude analysis on the NS equations. The resulting Boundary Layer (BL) equations are widely used for many high Reynolds number flows. One of the attractive

features of the BL equations is that they are parabolic. This implies that the solution can be marched in the streamwise direction without iteration.

Another simplified form of the NS equations is the Approximate Navier-Stokes (ANS) equations. The ANS equations assume that only the viscous terms with derivatives in the streamwise direction are small; all other terms are retained. The ANS equations fall between the Navier-Stokes and the Boundary Layer equations in terms of accuracy. They are useful because they are partially parabolized in the case of subsonic flow and are a mixed set of parabolic/hyperbolic equations for supersonic flow [1]. The parabolized equations allow for forward marching in the streamwise direction. For subsonic flow, forward marching is still possible, however, several iterations may be necessary to achieve convergence since the equations still contain elliptic inertia type terms.

Approximate forms of the NS equations are particularly useful when used in recently developed zonal techniques. These techniques divide the flow region into distinct zones, each having a particular set of assumptions about the flow. For example, when the Reynolds number is large the flow region can be broken up into a viscous region (where the ANS or BL equations can be used) and an inviscid region where a greatly simplified inviscid model is used. If the viscous region is small in comparison with the inviscid region the

computational savings can be substantial. This is true because the mathematical model for the viscous flow will be solved over a relatively small region while the larger inviscid region uses a simple inviscid code. A coupling scheme is employed in the zonal technique to insure compatibility between the two regions. The iteration of the boundary condition at the interface of the two regions is the mechanism through which the viscous and inviscid flow regions interact. There are many approaches available for solving such problems. The interacting boundary layer theory (IBLT) was used by Carter [2], Vatsa et. al.[3], Edwards and Carter [4] and Houwink and Veldman [5] to solve the viscous/inviscid problem. In the IBLT, the viscous region is represented by the boundary layer equations; the inviscid flow can be represented in a number of different ways depending upon the flow configuration and the Mach number. Rubin et. al.[6] and Swanson et. al.[7] used a composite velocity representation of the inviscid and viscous flow regions. Halim and Hafez [8-9] solved the viscous and the inviscid regions using a semi-implicit coupling technique. More recent efforts were also successful using a fully implicit coupling method to obtain efficient solutions [10-11] for viscous/inviscid problems.

Any numerical method developed must be able to generate regular solutions in the event of an adverse pressure gradient. If separation occurs there is a restriction on what can be used as the boundary condition to insure regular behavior. It is known that the solution of the boundary layer equations with a prescribed pressure gradient results in singularity at the point of separation [12]. The singularity at the separation point is independent of the form of the equations (i.e. integral or differential). The work of Carter [13] showed that regular solutions can be obtained with an inverse approach in which either the displacement thickness or the skin friction is specified. In addition, the criterion of Meksyn [14] states that if U_e (the velocity at the outer edge of the viscous layer) did not include any correction due to the interaction between the viscous and inviscid regions, then the boundary layer solution would be singular at the point of separation.

In the present work, three methods were developed to solve for subsonic flows with viscous/inviscid interaction; a finite difference method, an integral boundary layer method, and a Hilbert integral method. The presence of the boundary layer is assumed to affect the solution of the inviscid flow region.

In the first method, the finite difference form of the ANS equations are solved in the viscous region while Laplace's equation written in terms of the stream function is solved in the inviscid region. A coupling scheme is developed to find the stream function at the interface. One cycle yields a new stream function distribution as opposed to reference [4], where many cycles are needed. Each cycle is equivalent to repeated Successive Line Over-relaxation (SLOR) sweeps. Edwards and Carter [4] used repeated SLOR sweeps for each new displacement thickness to determine the solution in the inviscid region. The critical issues of this method are the efficiency of the viscous solver and the development of the fully implicit coupling.

The second method uses a finite difference scheme for the inviscid region and an integral approach for the boundary layer equations in the viscous region. The displacement thickness now represents the shape of a displaced body over which the flow is inviscid. A shear transformation is performed in the inviscid region to allow for a uniform grid in the computational domain. The inviscid solution will produce U_e and V_e. The Integral Boundary Layer (IBL) equations are written in terms of V_e, resulting in two equations and two unknowns (δ and C_f) when a velocity profile is assumed. The displacement thickness can now be found and used as the next boundary condition to the inviscid solver. This cycle continues until convergence is achieved.

The ultimate goal of the IBL method is the development of an integrated solver for the entire flow field. The key to finding an integrated solver is to find an efficient method for defining the displaced body.

The third method solves the finite difference form of the boundary layer equations using the inverse mode. The streamwise velocity at the boundary layer edge, U_e, is written as the sum of the inviscid velocity plus a term which accounts for the viscous effects. The viscous region is solved to obtain $U_{e,bl}$. The Hilbert integral finds the correction to U_e based on the displacement thickness used as the input to the boundary layer equations. The resulting velocity, $U_{e,h}$, will be compared with $U_{e,bl}$. If $U_{e,h}$ and $U_{e,bl}$ are not equal within a set tolerance, then the method continues until convergence is achieved.

The model problem chosen to develop the current methods is Howarth [15] flow over a flat plate, which prescribes a piecewise linear external velocity profile as shown in Figure 1. The variation of the external velocity with x implies a pressure gradient in the streamwise direction. Flow separation can occur if the corner position X_0 is chosen correctly. Briley [16] solved this flow using the full Navier-Stokes equations, achieving separation with X_0=0.2 for R_e=20800. The current work will also use X_0=0.2 and R_e=20800.

The flow region, depicted in Figure 2, consists of a two-dimensional rectangular area where the flow is subsonic everywhere in the field. The upstream boundary begins at a non-dimensional length of x=0.05 along the flat plate where x is in the streamwise direction and Y is in the direction normal to the plate. The downstream boundary is at x=0.489 after Briley. The outer boundary used in the present work was Y = 7.23 where Briley used Y = 5.4 as the outer boundary. The difference in the two outer boundaries is present to allow for adequate grid resolution in the current inviscid solver while also assuring that the interface is positioned above the boundary layer.

Results of the three methods are presented and compared to existing work. Solution accuracy, memory requirements, and computation time are discussed and recommendations for further study are given.

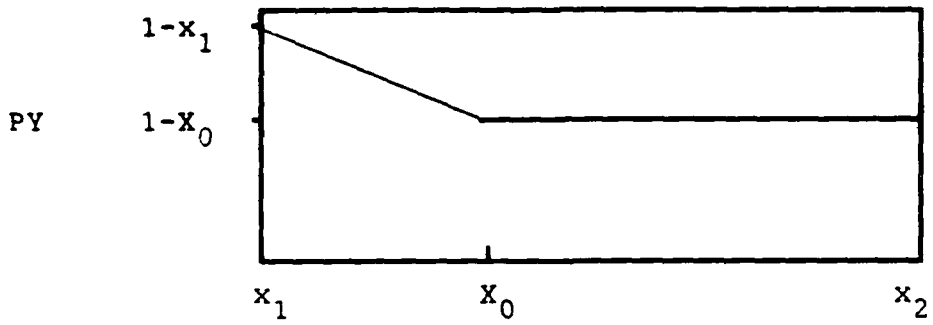

Figure 1. Howarth velocity profile

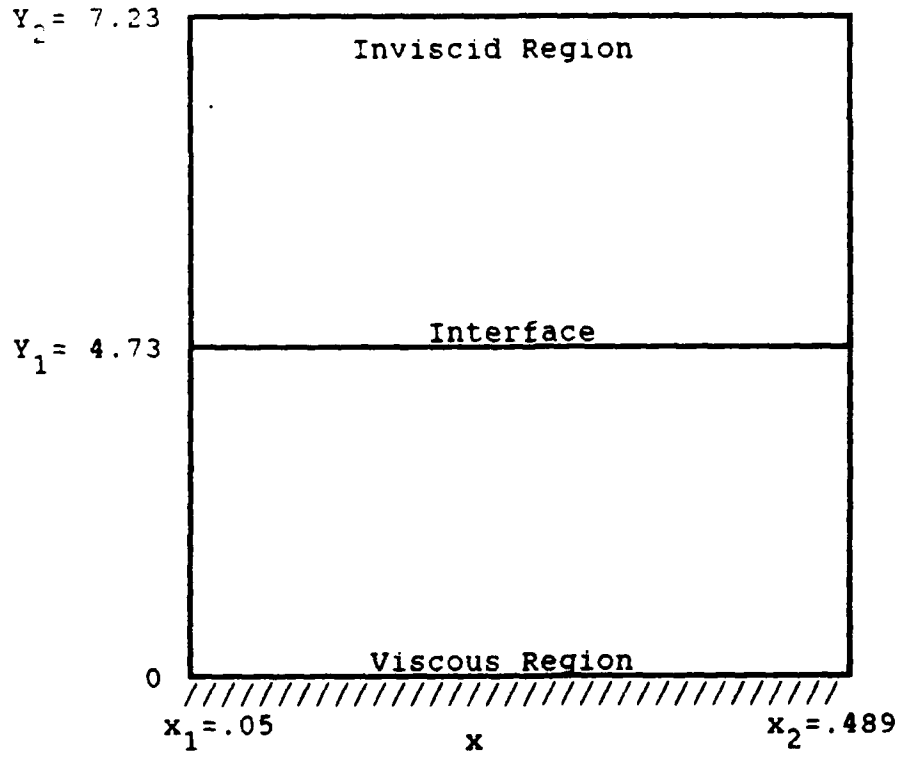

Figure 2. Flow Boundaries

II Analysis

Approximate Navier-Stokes (ANS) Equations

The development of the ANS and IBL equations will start from the full Navier-Stokes (NS) equations. For 2-D incompressible, steady flow in the absence of body forces [17] the NS equations in dimensional form simplify to

$$u_x + v_y = 0 \tag{2.1}$$

$$uu_x + vu_y = -p_x/\rho + \nu\,(u_{xx} + u_{yy}) \tag{2.2}$$

$$uv_x + vv_y = -p_y/\rho + \nu\,(v_{xx} + v_{yy}) \tag{2.3}$$

where

u = velocity in x (streamwise) direction

v = velocity in y (normal) direction

p = pressure

ρ = fluid density (constant)

ν = fluid kinematic viscosity (constant)

The subscripts denote partial differentiation with respect to that variable. The energy equation is not considered here since Eqns (2.1)-(2.3) and the energy equation are uncoupled for incompressible flow. Eqs (2.1)-(2.3) can be put in nondimensional form by defining the quantities

$$u' = u/u_\infty \qquad v' = v/v_\infty$$

$$x' = x/L \qquad y' = y/L$$

$$p' = p/\rho u_\infty^2 \tag{2.4}$$

where

u_∞ = free stream velocity

L = characteristic length

Applying Eqn (2.4) to Eqns (2.1)-(2.3) and dropping the primes yields

$$u_x + v_y = 0 \tag{2.5}$$

$$uu_x + vu_y = -p_x + R_e^{-1}(u_{xx} + u_{yy}) \tag{2.6}$$

$$uv_x + vv_y = -p_y + R_e^{-1}(v_{xx} + v_{yy}) \tag{2.7}$$

where the Reynolds number R_e is defined by

$$R_e = u_\infty L/\nu \tag{2.8}$$

Equations (2.5)-(2.7) are the NS equations written in nondimensional form.

The BL equations are obtained by considering the scaling law of the relative magnitudes of velocity components in the thin region. This leads to an estimate of the nondimensional boundary layer thickness

$$\delta \sim R_e^{-1/2} \tag{2.9}$$

where the symbol $\sim$ implies order of magnitude. This is a fundamental result of boundary layer analysis. Notice that for very large R_e the order of magnitude of the boundary layer thickness is much less than unity. Therefore terms in the NS equations that are found to be of order of magnitude δ can be neglected compared to terms that are of order unity. First consider Eq (2.5), the continuity equation. The u

velocity and the streamwise coordinate x are clearly of order unity by definition. This implies that

$$v_y \sim 1 \tag{2.10}$$

and since the normal direction y is of order δ, then

$$v \sim \delta \tag{2.11}$$

Since R_e^{-1} is of order δ^2 from Eq (2.9), the order of magnitude of each term in Eqns (2.6) and (2.7) can be determined. The result is that the x momentum equation (2.6) contains terms of order unity except for the term

$$R_e^{-1} u_{xx}$$

which is of order δ^2. The y momentum equation (2.7) is found to have all terms of order δ except for the term

$$R_e^{-1} v_{xx}$$

which is of order δ^3. These two terms can be neglected compared to the relative magnitude of the remaining terms. The resulting set of equations is

$$u_x + v_y = 0 \tag{2.12}$$

$$uu_x + vu_y = -p_x + R_e^{-1} u_{yy} \tag{2.13}$$

$$uv_x + vv_y = -p_y + R_e^{-1} v_{yy} \tag{2.14}$$

The Prandtl boundary layer equations consist of Eqns (2.12) and (2.13). Since all terms in Eq (2.14) are of order δ, it is omitted in the classic boundary layer approximation. The ANS equations retain equation (2.14), allowing for a change in pressure normal to the streamwise direction. These equations will now be written in terms of the stream function Ψ and the vorticity ω.

The stream function Ψ is defined for 2-D, incompressible flow such that

$$u = \Psi_y \tag{2.15}$$

$$v = -\Psi_x \tag{2.16}$$

and the vorticity, ω, is defined as

$$\omega = v_x - u_y \tag{2.17}$$

Notice that the continuity equation (2.12) is automatically satisfied by the definition of Ψ. The pressure can be eliminated from Eqns (2.13) and (2.14) by taking the partial derivative of Eq (2.13) with respect to y and subtracting the partial derivative of (2.14) with respect to x. Four of the resulting terms are eliminated by the continuity equation, leaving

$$u(v_{xx} - u_{xy}) + v(v_{xy} - u_{yy}) = R_e^{-1}(v_{xyy} - u_{yyy}) \tag{2.18}$$

which can be simplified to

$$\boxed{\Psi_y \omega_x - \Psi_x \omega_y - R_e^{-1} \omega_{yy} = 0} \tag{2.19}$$

by taking derivatives of Eq (2.17) and substituting them into Eq (2.18). The velocities u and v were also expressed in terms of Ψ from Eqns (2.15) and (2.16). The vorticity can also be expressed in terms of Ψ in Eq (2.17) to obtain

$$\boxed{\Psi_{xx} + \Psi_{yy} + \omega = 0} \tag{2.20}$$

Equations (2.19) and (2.20) are the ANS equations for 2-D incompressible flow written in terms of Ψ and ω. These equations are the model for the viscous region in the first

method, where finite difference representations are used. The inviscid model is obtained directly from Eqn (2.20), where the vorticity is zero. The resulting equation is simply

$$\boxed{\Psi_{xx} + \Psi_{yy} = 0} \qquad (2.21)$$

Integral Equations

The Integral Boundary Layer (IBL) equation can be obtained by integrating the dimensional form of the x momentum equation

$$uu_x + v\,u_y = -p_x/\rho + \nu\,u_{yy} \qquad (2.22)$$

from y=0 to y=δ. The pressure term can be expressed in terms of the velocity at the edge of the boundary layer, U_e, by considering the boundary conditions

$$u|_{y=\delta} = U_e$$

$$u_y|_{y=\delta} = 0$$

$$u_{yy}|_{y=\delta} = 0$$

Imposing these conditions on Eq (2.22) results in

$$U_e\,dU_e/dx = -p_x/\rho \qquad (2.23)$$

Substitute Eq (2.23) into Eq (2.22) and integrate over the boundary layer to give

$$\int_0^\delta (uu_x + vu_y - U_e\,dU_e/dx)\,dy = \nu\int_0^\delta u_{yy}\,dy \qquad (2.24)$$

which simplifies to

$$\int_0^{\delta} (uu_x + vu_y - U_e\, dU_e/dx)\, dy = -\tau_w/\rho \qquad (2.25)$$

where τ_w is the shear stress at the wall, defined by

$$\tau_w = \mu\, u_y|_{y=0} \qquad (2.26)$$

The normal velocity component, v, can be replaced in Eq (2.25) by

$$v = -\int_0^y u_x\, dy \qquad (2.27)$$

which is a result obtained by integrating the continuity equation. Substitute Eq (2.27) into Eq (2.25) to obtain

$$\int_0^{\delta} (uu_x - u_y \int_0^y u_x\, dy - U_e\, dU_e/dx)\, dy = -\tau_w/\rho \qquad (2.28)$$

Integrate by parts to obtain the second term

$$\int_0^{\delta} (u_y \int_0^y u_x\, dx)\, dy = U_e \int_0^{\delta} u_x\, dy - \int_0^{\delta} uu_x\, dy \qquad (2.29)$$

and substitute into Eq (2.28) to get

$$\int_0^{\delta} (2uu_x - U_e u_x - U_e\, dU_e/dx)\, dy = -\tau_w/\rho \qquad (2.30)$$

which after rearrangement yields

$$\int_0^{\delta} \partial/\partial x(u(U_e - u))\, dy + dU_e/dx \int_0^{\delta} (U_e - u)\, dy = \tau_w/\rho \qquad (2.31)$$

The displacement thickness δ^* and momentum thickness θ are defined as

$$U_e\, \delta^* = \int_0^{\delta} (U_e - u)\, dy \qquad (2.32)$$

and

$$U_e^2\, \theta = \int_0^{\delta} u(U_e - u)\, dy \qquad (2.33)$$

Substitute Eqns (2.32) and (2.33) into (2.31) to obtain

$$d/dx\ (U_e^2\theta) + \delta^*\ U_e\ dU_e/dx = \tau_w/\rho \qquad (2.34)$$

Now cast Eq (2.34) into nondimensional form by introducing the skin friction coefficient C_f, which has the definition

$$C_f = \frac{2\ \tau_w}{\rho U_\tau^2} \qquad (2.35)$$

Expanding the first term of Eq (2.34) and writing the entire equation in nondimensional form gives the final form of the integral boundary layer equation

$$\boxed{d\theta/dx + \frac{\theta}{U_e}\ dU_e/dx\ (2 + \delta^*/\theta) = C_f/2} \qquad (2.36)$$

An alternative form to Eqn (2.36) is found by multiplying it by U_e^2 and rearranging to get

$$\boxed{d/dx[\ U_e^2\theta\ ] + U_e\ (dU_e/dx)\ \delta^* = U_e^2\ C_f/2} \qquad (2.37)$$

Eqn (2.37) is used in the second method. The unknowns are C_f, θ, and δ^*. By assuming a velocity profile, the unknowns can be reduced to two (C_f and δ). The second equation is a form of the continuity equation

$$u_x + v_y = 0$$

Add and subtract the term dU_e/dx and rearrange to get

$$v_y = dU_e/dx - dU_e/dx - u_x \qquad (2.38)$$

Integrating this equation from y=0 to y=δ and using Eqn (2.32) results in

$$\boxed{V_e = d/dx \left[U_e \delta^* \right] - \delta \, dU_e/dx} \qquad (2.39)$$

Equations (2.37) and (2.39) are solved simultaneously.

Representation of the inviscid flow using a panel method

The Hilbert Integral represents the correction to the inviscid velocity U_e due to the effects of the displacement thickness. To find an expression for this correction δu, one can consider a line of source distribution q(x) at y=0 that is constructed such that the resulting flow takes place over a displaced body defined by the displacement thickness $\delta^*(x)$. Figure 3 shows a typical source distribution that results in flow over the body defined by $\delta^*(x)$. The source strength is defined by the constant mass flow rate it generates. By considering a circular control volume centered about the source, the strength can be shown to be related to the flow velocity at a distance r from the source by

$$q(\xi) \, d\xi = 2\pi r \, V \qquad (2.40)$$

The x component of velocity $d(\delta u)$ for a source of strength $q(\xi) \, d\xi$ located at $x=\xi$ (Fig. 3) is simply

$$d(\delta u) = V \cos \theta = q(\xi) \, d\xi \, (x - \xi) \, / \, 2\pi r^2 \qquad (2.41)$$

where

$$r^2 = (x - \xi)^2 + \delta^{*2} \qquad (2.42)$$

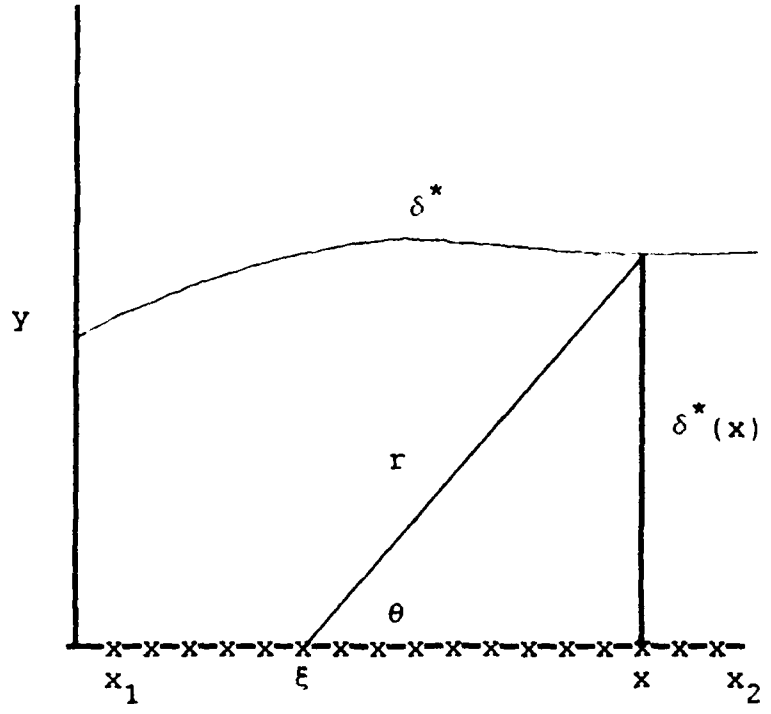

Figure 3. Source distribution geometry

The total δu considering the range between x_1 and x_2 is

$$\delta u(x) = \int_{x_1}^{x_2} q(\xi)\ (x - \xi)\ /\ 2\pi r^2\ d\xi \qquad (2.43)$$

Integrating Eqn (2.43) from zero to y will give the stream function Ψ. This integration results in

$$\Psi = \int_{x_1}^{x_2} \left[\ q(\xi)\ \tan^{-1}(y/(x-\xi))\ /\ 2\pi\ \right] d\xi + C \qquad (2.44)$$

The relation between Ψ at $y=\delta^*$ and Ψ at $y=0$ can be approximated by considering a Taylor series expansion of Ψ, where

$$\Psi(x,0) \cong \Psi(\delta^*) - \Psi_{y|y=\delta^*}\ (\delta^*) = -\ U_e\ \delta^* \qquad (2.45)$$

since $\Psi_{y|y=\delta^*} = U_e$ and $\Psi(\delta^*) = 0$. Differentiating Eqn (2.45) with respect to x gives

$$d\Psi(x,0)/dx = -d(U_e\delta^*)/dx \qquad (2.45a)$$

Differentiating Eqn (2.44) with respect to x and taking the limit as y goes to zero and equating the result to Eqn (2.45a) will give the simple relation

$$q(\xi) = 2\ d(U_e\delta^*)/d\xi \qquad (2.46)$$

Substituting Eqn (2.46) into Eqn (2.43) gives the final Hilbert integral expression for δu as

$$\boxed{\delta u(x) = \pi^{-1} \int_{x_1}^{x_2} \left[d(U_e\delta^*)/d\xi\right]\ (x-\xi)/r^2\ \ d\xi} \qquad (2.47)$$

The streamwise velocity $U_{e,h}$ is calculated from

$$U_{e,h}(x) = PY(x) + \delta u(x) \qquad (2.48)$$

which includes the correction δu due to the viscous effects.

Boundary Conditions

The boundary conditions will now be discussed in general for the three methods. Figure 4 shows the computational domain and governing equations for the viscous and inviscid regions. The domain consists of a 2-D rectangular region with subsonic flow throughout. Boundary conditions for Ψ and ω are specified at each of the boundaries (a)-(e).

At the outer flow boundary (a) the velocity is specified by Howarth's profile.

$$PY(x) = 1 - x \quad , \quad \text{for } x < X_0$$
$$PY(x) = X_0 \quad , \quad \text{for } x \geq X_0 \qquad (2.49)$$

where X_0 is chosen to be 0.2 after Briley [16].

The inlet flow (b) is assumed known from boundary layer theory. Howarth [15] solved this flow using series representations to obtain solutions up to the separation point. The resulting streamwise velocity distribution is compared in Figure 5 to the distribution obtained from boundary layer code [18]. The variable ETA in Figure 5 is defined as η, where

$$\eta = 0.5\ y\ (R_e/x_1)^{1/2} \qquad (2.50)$$

Note the excellent agreement between the data. The velocity obtained from the boundary layer code can be integrated with respect to the normal direction to obtain Ψ at the inlet.

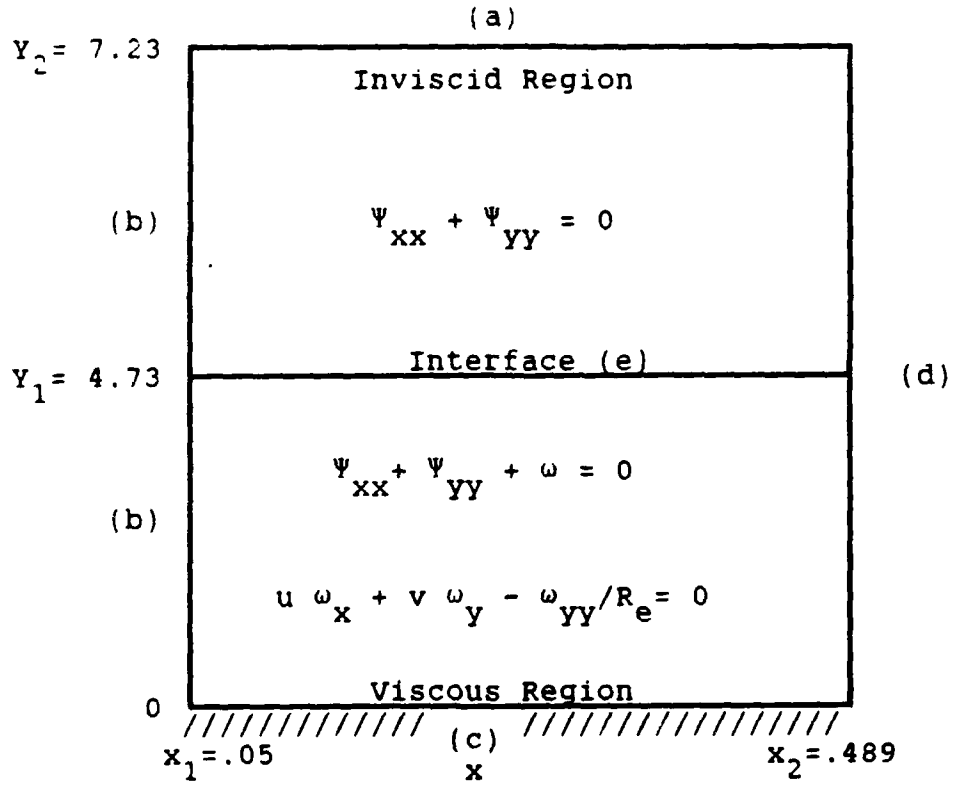

Figure 4. Flow boundaries and governing equations

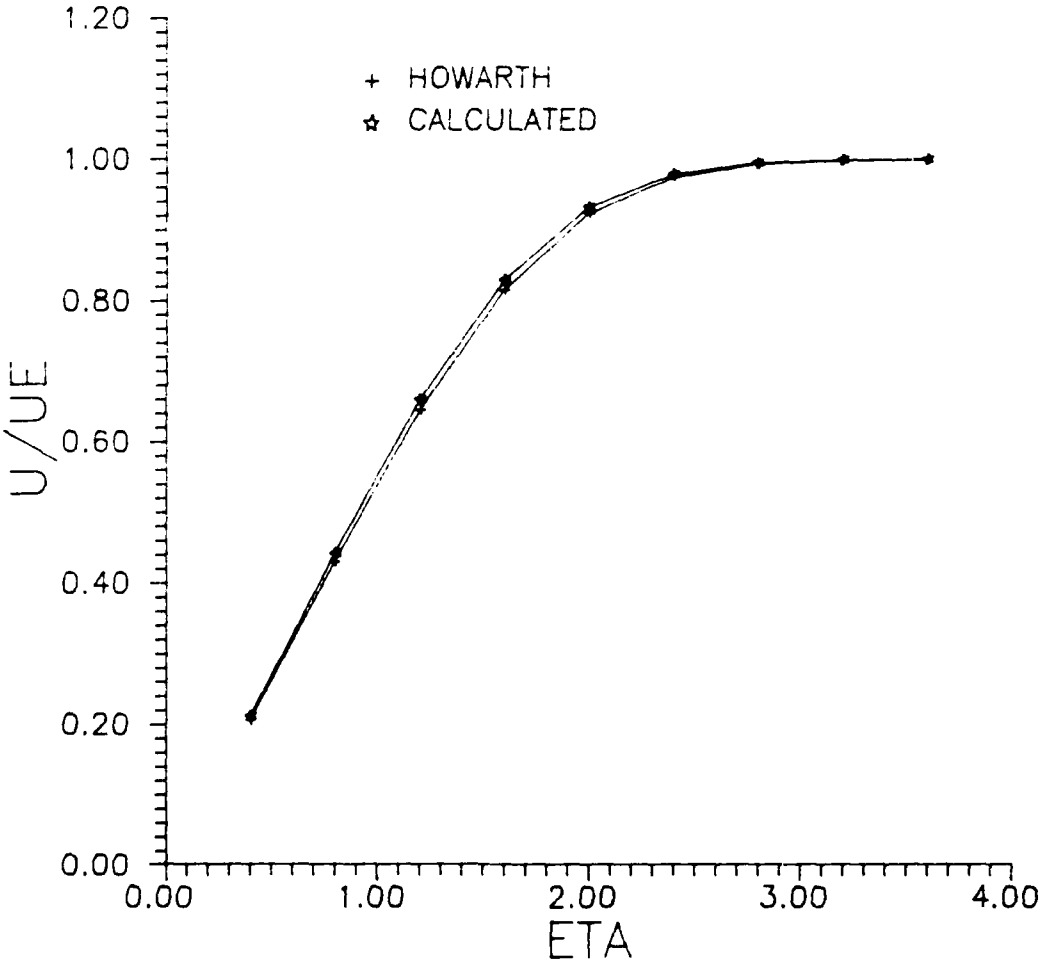

Figure 5. Comparison of Howarth velocity profile to boundary layer code

The inlet vorticity is obtained from Eqn (2.20) assuming $\Psi_{xx}=0$ in the boundary layer, resulting in

$$\omega|_{x=x1} = -\Psi_{yy}|_{x=x1} \tag{2.51}$$

The no slip condition prevails at (c), where

$$u|_{y=0} = \Psi_{y}|_{y=0} = 0 \tag{2.52}$$

and

$$v|_{y=0} = -\Psi_{x}|_{y=0} = 0 \tag{2.53}$$

and therefore

$$\Psi|_{y=0} = 0 \tag{2.54}$$

Also, since $\Psi=0$ everywhere along the plate surface

$$\Psi_{xx}|_{y=0} = 0 \tag{2.55}$$

and therefore the vorticity is given by

$$\omega|_{y=0} = -\Psi_{yy}|_{y=0} \tag{2.56}$$

from equation (2.20).

At the downstream location (d) a boundary condition on Ψ alone is required since the ANS equations contain the elliptic term Ψ_{xx}. If the full Navier-Stokes equations were used, the term ω_{xx} would be present in Eqn (2.19), requiring a downstream boundary condition for the vorticity in the viscous region. The boundary condition on Ψ is obtained assuming that (d) is far downstream from the pressure gradient disturbance. Uniform flow is assumed where

$$v|_{x=x2} = -\Psi_{x}|_{x=x2} = 0 \tag{2.57}$$

At the interface (e) the stream function is obtained directly from the coupling scheme for the finite difference method. The integral and Hilbert methods assume that the interface represents the displaced body over which the flow is inviscid. For this case $\Psi=0$ along the interface. The vorticity is assumed to be zero along the interface. This represents a departure from normal boundary layer type conditions where the free stream velocity is allowed to be satisfied asymptotically at an infinite distance normal to the wall [16]. In the present work, these conditions are imposed at a finite distance from the body surface.

The placement of the interface from the wall can be quite important. Briley's solution to the present case of $X_0=0.2$ shows that the maximum value of δ^* is about 0.015. For the simple case of a linear velocity distribution, the boundary layer thickness is equal to twice the displacement thickness [17]. Thus, for the present work the location of the interface should be at or greater than approximately y=.03, which corresponds to Y = 4.32 for R_e = 20800.

III Methods of Solution

Method I

Solution Procedure. The governing equations for this method are the ANS equations (2.19) and (2.20) for the viscous region and Laplace's equation (2.21) in the inviscid region. The flow is initialized everywhere by the inlet conditions. The finite difference form of Eqns (2.20) and (2.19), respectively, can be written as

$$A_{1j}\Psi_{i,j-1} + B_{1j}\Psi_{i,j} + C_{1j}\Psi_{i,j+1} + D_{1j}\omega_{i,j-1} + E_{1j}\omega_{i,j} + F_{1j}\omega_{i,j+1} = RHS_{1,j} \quad (3.1)$$

and

$$A_{2j}\Psi_{i,j-1} + B_{2j}\Psi_{i,j} + C_{2j}\Psi_{i,j+1} + D_{2j}\omega_{i,j-1} + E_{2j}\omega_{i,j} + F_{2j}\omega_{i,j+1} = RHS_{2,j} \quad (3.2)$$

Where the indices i,j represent the computational domain grid points in the streamwise and normal directions respectively. The finite difference form for Eqn (2.21) can be written as

$$A_{3j}\Psi_{i,j-1} + B_{3j}\Psi_{i,j} + C_{3j}\Psi_{i,j+1} = RHS_{3,j} \quad (3.3)$$

The calculation of the above coefficients and right hand sides is the subject of the next two sections. The results can be found in Eqns (3.18)-(3.21) for Eqn (3.3). The coefficients for Eqn (3.1) will be similar to the coefficients for equation (3.3) since the two equations differ only by the vorticity term.

The coefficients for Eqn (3.2) can be found in Eqns (3.44)-(3.50). For now, only the method of solution is discussed.

Successive Line Over-Relaxation (SLOR) is used in both regions. The solution procedure, depicted in Figure 6, starts at the inlet and marches downstream. At each i location the coefficients of Eqns (3.1)-(3.3) are found. For the inviscid region this results in a tridiagonal system of equations which can be solved using a form of the Thomas algorithm [19] described in Appendix A. This algorithm puts a tridiagonal matrix of equations in upper triangular form and then performs back substitution to find the solution directly. From this algorithm, the solution at the interface J can be written in terms of the solution at the J+1 point by the relation

$$\Psi_{i,J+1} = \beta_{i,J+1} \Psi_{i,J} + \gamma_{i,J+1} \tag{3.4}$$

Where $\beta_{i,J+1}$ and $\gamma_{i,J+1}$ are recurrence coefficients. The boundary conditions are enforced by the definition of the coefficients A_3, B_3, C_3 , and RHS_3 at the boundaries. For the viscous region Eqns (3.1) and (3.2) result in a block 2x2 set of equations that is solved using a special form of the Thomas algorithm for two partial differential equations. This algorithm is also described in Appendix A.

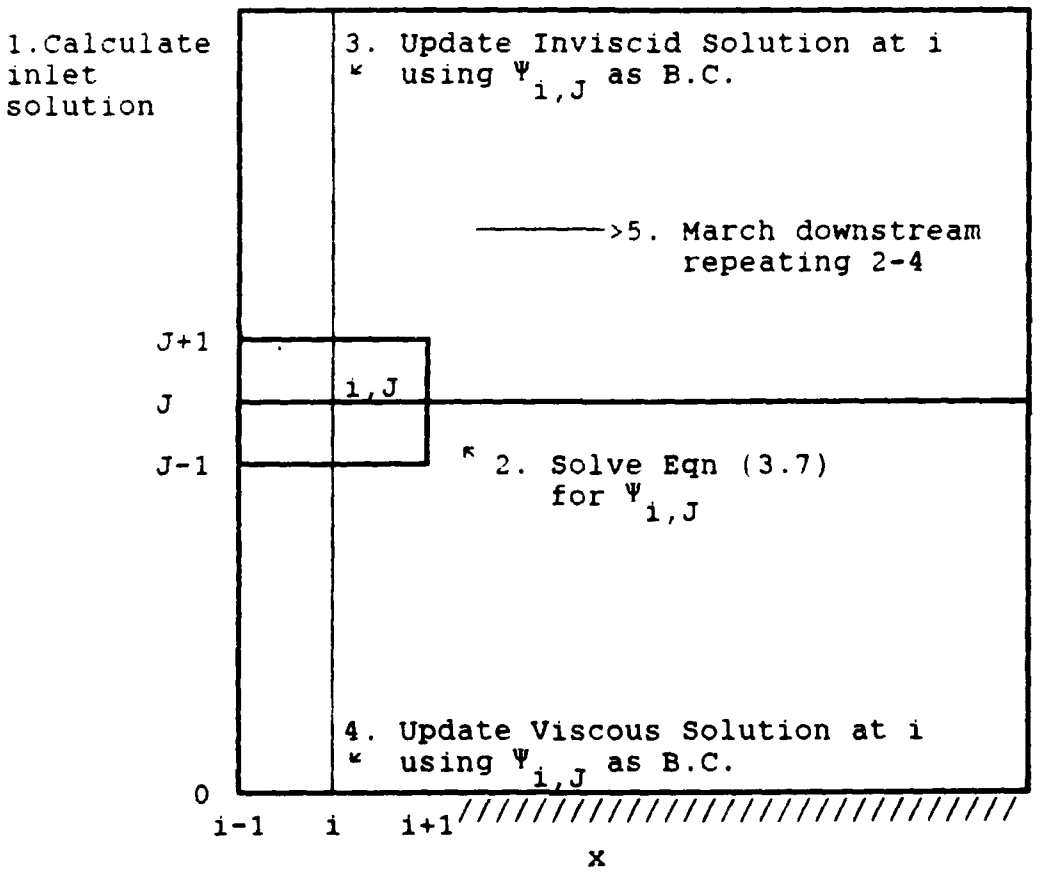

Figure 6. Solution procedure for Method I

The solution for the viscous equations will have the form

$$\Psi_{i,j} = R_{1,j}\,\Psi_{i,j+1} + S_{1,j}\,\omega_{i,j+1} + T_{1,j} \qquad (3.5)$$

$$\omega_{i,j} = R_{2,j}\,\Psi_{i,j+1} + S_{2,j}\,\omega_{i,j+1} + T_{2,j} \qquad (3.6)$$

where $R_{1,j}$ ... $T_{2,j}$ are the recurrence coefficients. With Eqns (3.4)-(3.6) the solution to both the viscous and inviscid regions can be found given all of the boundary conditions. A crucial element of the solution process, however, is the coupling scheme between the two regions. The governing equations at the interface is given by Eqn (2.21), since the vorticity is assumed to be zero. The finite difference equations at the interface j=J has the form

$$A\,\Psi_{i-1,J} + B\,\Psi_{i,J} + C\,\Psi_{i+1,J} + D\,\Psi_{i,J+1} + E\,\Psi_{i,J-1} = 0 \qquad (3.7)$$

where the coefficients A-E are known. The goal is to be able to solve for $\Psi_{i,J}$ in Eqn (3.7). The value of $\Psi_{i-1,J}$ is known because the solution is sweep downstream. The value of $\Psi_{i+1,J}$ is approximated to the value from the previous level. Note that this assumption is valid since the difference in Ψ between successive levels goes to zero as the solution converges. The remaining unknowns are $\Psi_{i,J}$, $\Psi_{i,J+1}$, and $\Psi_{i,J-1}$. Using Eqns (3.4)-(3.6) the terms $\Psi_{i,J+1}$ and $\Psi_{i,J-1}$ can be written in terms of $\Psi_{i,J}$ from the recurrence. Since the vorticity is assumed to be zero at the interface, the recurrence relation for Ψ given by Eqn (3.5) can be reduced at the interface to

$$\Psi_{1,J-1} = R_{1,J-1}\,\Psi_{i,J} + T_{1,J-1} \qquad (3.8)$$

Substituting Eqns (3.4) and (3.8) into Eqn (3.7) results in one equation with one unknown. The stream function at the interface, $\Psi_{i,J}$, is calculated and used as the new boundary condition. The solution in the inviscid region is calculated directly since it uses a non-recurrence form of the Thomas algorithm. See Appendix A. Eqns (3.5) and (3.6) are used to generate the solution in the viscous region once the recurrence coefficients are known. Both solutions use Ψ at the interface calculated from Eqn (3.7) as a boundary condition. The algorithm moves downstream to the next i location where the process repeats until i reaches IMAX-1. Residuals are then calculated and compared to a tolerance value. If the residual tolerance is not satisfied the iterations continue back at i=2 and the solution process continues until convergence is achieved.

Inviscid Region. The model for the inviscid region is Laplace's equation

$$\Psi_{xx} + \Psi_{yy} = 0 \qquad (3.9)$$

Appendix B contains all of the finite difference forms of the derivatives; allowing for a non-uniform grid. The coordinates (x,y) represent the physical domain and (ξ,η) represent the uniform computational domain. The indices of the uniform grid are denoted by i in the ξ direction and j in the η direction.

Eqn (3.9) written in finite difference form becomes

$$A_j^* \Psi_{i,j+1} + B_j^* \Psi_{i,j} + C_j^* \Psi_{i,j-1} + D_j^* \Psi_{i+1,j} + E_j^* \Psi_{i-1,j} = 0 \qquad (3.10)$$

where,

$$A_j^* = \eta_{y,j}\, \eta_{y,j+1/2} / \Delta\eta^2 \qquad (3.11)$$

$$B_j^* = -\eta_{y,j} (\eta_{y,j+1/2} + \eta_{y,j-1/2}) / \Delta\eta^2 - \xi_{x,j} (\xi_{x,j+1/2} + \xi_{x,j-1/2}) / \Delta\xi^2 \qquad (3.12)$$

$$C_j^* = \eta_{y,j}\, \eta_{y,j-1/2} / \Delta\eta^2 \qquad (3.13)$$

$$D_j^* = \xi_{x,j}\, \xi_{x,j+1/2} / \Delta\xi^2 \qquad (3.14)$$

$$E_j^* = \xi_{x,j}\, \xi_{x,j-1/2} / \Delta\xi^2 \qquad (3.15)$$

as given in Appendix B. It is implied that the stream function Ψ in Eqn (3.10) is written at the unknown level denoted as n+1, whereas n represents the current level. The n+1 level is implied throughout this report. Terms at the current level will carry the n superscript. Rearrange Eqn (3.10) to obtain

$$\Psi_{i,j} = -[A_j^* \Psi_{i,j+1} + C_j^* \Psi_{i,j-1} + D_j^* \Psi_{i+1,j} + E_j^* \Psi_{i-1,j}] / B_j^* \qquad (3.16)$$

Relaxation is now introduced to enhance the convergence of the solution. The relaxation parameter W is defined such that Ψ at the unknown level is written as

$$\Psi_{i,j} = (1 - W) \Psi_{i,j}^{n} + W \Psi_{i,j} \qquad (3.17)$$

Notice that when W = 1, Eqn (3.17) becomes a simple identity with no relaxation of the solution. Over-relaxation (W > 1) can be used to accelerate the convergence if the solution is relatively stable. Under-relaxation (W < 1) is used mainly to maintain numerical stability in the iteration process. In this case more of the solution at the current value of Ψ is used to help stabilize the solution. Substituting Eqn (3.16) into Eqn (3.17) and rearranging gives Eqn (3.3) rewritten as

$$A_{3j}\Psi_{i,j-1} + B_{3j}\Psi_{i,j} + C_{3j}\Psi_{i,j+1} = RHS_{3,j}$$

where,

$$A_{3j} = W\, C_j^* / B_j^* \tag{3.18}$$

$$B_{3j} = 1 \tag{3.19}$$

$$C_{3j} = W\, A_j^* / B_j^* \tag{3.20}$$

$$RHS_{3,j} = (1 - W)\, \Psi_{i,j}^n - W\, D_j^*\, \Psi_{i+1,j} / B_j^* - W\, E_j^*\, \Psi_{i-1,j} / B_j^* \tag{3.21}$$

All of the terms in RHS_3 are known. The $\Psi_{i,j}^n$ term is known since it is at the current level. The stream function at i-1 is known because the solution is marched downstream. The stream function at i+1 is assumed to be equal to $\Psi_{i+1,j}^n$ as an approximation. The boundary conditions are imposed by redefining the coefficients of Eqn (3.3) at the boundaries.

The condition at the outer boundary is given by Eqn (2.49), rewritten as

$$\Psi_y|_{y=y2} = PY(x) \tag{3.22}$$

where PY(x) is defined by Howarth's velocity profile as

$$PY(x) = 1 - x \quad , \text{ for } x < X_0 \tag{3.23}$$

$$PY(x) = X_0 \quad , \quad \text{for } x \geq X_0 \tag{3.24}$$

Writing Eqn (3.22) in finite difference form gives

$$\eta_{yj2} \left(\Psi_{i,j2} - \Psi_{i,j2-1} \right) / \Delta\eta = PY(x) \tag{3.25}$$

which can be written as

$$\Psi_{i,j2} = \Psi_{i,j2-1} + \left(PY(x)\, \Delta\eta \,/\, \eta_{yj2} \right) \tag{3.26}$$

Substituting this equation into Eqn (3.3) written at j=j2-1 gives

$$A_{3,j2-1}\, \Psi_{i,j2-2} + B_{3,j2-1}\, \Psi_{i,j2-1} +$$

$$C_{3,j2-1} \left(\Psi_{i,j2-1} + (PY(x)\, \Delta\eta \,/\, \eta_{yj2}) \right) = RHS_{3,j2-1} \tag{3.27}$$

which can be cast back into the form of Eqn (3.3). The resulting coefficients are given in terms of their previous definitions as

$$A_{3,j2-1} = A_{3,j2-1}$$

$$B_{3,j2-1} = B_{3,j2-1} + C_{3,j2-1}$$

$$RHS_{3,j2-1} = RHS_{3,j2-1} - C_{3,j2-1}\, PY(x)\, \Delta\eta \,/\, \eta_{yj2}$$

$$C_{3,j2-1} = 0 \tag{3.28}$$

where the equal sign above implies replacement of the terms as in the FORTRAN programming language. Also note that $C_{3,j2-1}$ is set to zero after calculating the other terms.

The boundary condition for Ψ at the interface is given by the solution to Eqn (3.7) as previously discussed. For this case the coefficients are found to be

$$B_{3,J+1} = B_{3,J+1}$$
$$C_{3,J+1} = C_{3,J+1}$$
$$RHS_{3,,J+1} = RHS_{3,J+1} - A_{3,J+1}\,\Psi_{1,J}$$
$$A_{3,J+1} = 0 \qquad (3.29)$$

With all of the coefficients known, the tridiagonal solver is used to generate the recurrence relation at the interface and to generate the solution for Ψ. The calculations follow the solution procedure discussed in the previous section.

Viscous Region. The viscous region is bounded by the lower plate surface (Y=0), the upstream and downstream boundaries at x=.05 and x=0.489 respectively, and the interface at Y=4.73. The ANS equations (2.19) and (2.20) are the mathematical model for this region. These equations are scaled in the vorticity to allow for the unknowns Ψ and ω to be of similar order of magnitude. Define the vorticity as

$$\omega = \omega / \omega^* \qquad (3.30)$$

where ω^* is the vorticity at the plate at x=0.05. This scaling only affects Eqn (2.19) since ω^* will become a common factor in Eqn (2.20). The remaining discussion will assume the scaled form of the equations, written as

$$\Psi_{xx} + \Psi_{yy} + \omega\,\omega^* = 0 \qquad (3.31)$$
$$\Psi_y\,\omega_x - \Psi_x\,\omega_y - \omega_{yy}/R_e = 0 \qquad (3.32)$$

where the vorticity in (3.31) is the scaled vorticity. The convention used in the previous section where no superscript implies the unknown n+1 level and the superscript n implies the current level is retained here. Note that Eqn (3.32) is nonlinear since the n+1 level is implied on each term in the equation. Linearizing Eqn (3.32) results in

$$\psi_y^n \omega_x - \psi_x^n \omega_y + \omega_x^n \psi_y - \omega_y^n \psi_x$$
$$-\omega_{yy}/R_e = \psi_y^n \omega_x^n - \psi_x^n \omega_y^n \qquad (3.33)$$

The right hand side of Eqn (3.33) as well the n level terms are known from the current level. Finite difference expressions for ψ_x, ψ_y, ω_x, and ω_y are obtained from Appendix B. The finite difference form for Eqn (3.31) is exactly the result obtained from the previous section with the exception of the vorticity term. The resulting finite difference equation is simply Eqn (3.1)

$$A_{1j}\psi_{i,j-1} + B_{1j}\psi_{i,j} + C_{1j}\psi_{i,j+1} + D_{1j}\omega_{i,j-1} + E_{1j}\omega_{i,j}$$
$$+ F_{1j}\omega_{i,j+1} = RHS_{1,j} \qquad (3.1)$$

where the coefficients A_{1j}, B_{1j}, and C_{1j} are given by the right hand sides of Eqns (3.11)-(3.13) respectively and the remaining coefficients are

$$D_{1j} = 0 \qquad (3.34)$$

$$E_{1j} = 1 \qquad (3.35)$$

$$F_{1j} = 0 \qquad (3.36)$$

$$RHS_{1,j} = -D_j^* \psi_{i+1,j} - E_j^* \psi_{i-1,j} \qquad (3.37)$$

The finite difference form for Eqn (3.33) will now be addressed. The solution will be marched in the streamwise direction. Therefore, Ψ_x and ω_x are written as backward differences. The terms Ψ_y and ω_y are written as central differences. When Ψ_y is negative, the convective term $\Psi_y^n \omega_x$ will be written as upwind difference to honor the local streamwise direction in the reversed flow area. Now let

$$UP = 1/2 \left(\Psi_y^n + |\Psi_y|^n \right) \tag{3.38}$$

$$UM = 1/2 \left(\Psi_y^n - |\Psi_y|^n \right) \tag{3.39}$$

and notice that when $\Psi_y > 0$, UP equals Ψ_y and UM equals zero. When $\Psi_y < 0$, UP equals zero and UM equals $-\Psi_y$. The forward and backward finite difference forms of ω_x are

$$\omega_x|_i = \xi_{xi} \left(\omega_{i,j} - \omega_{i-1,j} \right) / \Delta\xi \tag{3.40}$$

$$\omega_x|_i = \xi_{xi} \left(\omega_{i+1,j} - \omega_{i,j} \right) / \Delta\xi \tag{3.41}$$

and therefore the convective term can be written as

$$\Psi_y^n \omega_x = UP\ \xi_{xi} \left(\omega_{i,j} - \omega_{i-1,j} \right) / \Delta\xi + UM\ \xi_{xi} \left(\omega_{i+1,j} - \omega_{i,j} \right) / \Delta\xi \tag{3.42}$$

Using Appendix B, Eqn (3.33) in finite difference form is

$$\begin{aligned} & UP\ \xi_{xi} \left(\omega_{i,j} - \omega_{i-1,j} \right) / \Delta\xi + UM\ \xi_{xi} \left(\omega_{i+1,j} - \omega_{i,j} \right) / \Delta\xi \\ & + \omega_x^n \left(P_{1j} \Psi_{i,j+1} + P_{2j} \Psi_{i,j} - P_{3j} \Psi_{i,j-1} \right) \\ & - \Psi_x^n \left(P_{1j} \omega_{i,j+1} + P_{2j} \omega_{i,j} - P_{3j} \omega_{i,j-1} \right) \\ & - \omega_y^n \left[\xi_{xi} \left(\Psi_{i,j} - \Psi_{i-1,j} \right) / \Delta\xi \right] \\ & - \left[Q_{1j} \omega_{i,j+1} - Q_{2j} \omega_{i,j} + Q_{3j} \omega_{i,j-1} \right] / R_e \\ & = \Psi_y^n \omega_x^n - \Psi_x^n \omega_y^n \end{aligned} \tag{3.43}$$

The terms P_1 ... Q_3 are given in Appendix B. Equation (3.43) is now cast into the form of Eqn (3.2), repeated here as

$$A_{2j}\Psi_{i,j-1} + B_{2j}\Psi_{i,j} + C_{2j}\Psi_{i,j+1} + D_{2j}\omega_{i,j-1} + E_{2j}\omega_{i,j} + F_{2j}\omega_{i,j+1} = RHS_{2,j} \quad (3.2)$$

by rearrangement of the terms in Eqn (3.43). The coefficients A_{2j} ... $RHS_{2,j}$ are given by

$$A_{2j} = - \omega_x^n P_{3j} \quad (3.44)$$

$$B_{2j} = \omega_x^n P_{2j} - \omega_y^n \xi_{xi} / \Delta\xi \quad (3.45)$$

$$C_{2j} = \omega_x^n P_{1j} \quad (3.46)$$

$$D_{2j} = \Psi_x^n P_{3j} - Q_{3j} / R_e \quad (3.47)$$

$$E_{2j} = \xi_{xi} (UP - UM) / \Delta\xi - \Psi_x^n P_{2j} + Q_{2j} / R_e \quad (3.48)$$

$$F_{2j} = -\Psi_x^n P_{1j} - Q_{1j} / R_e \quad (3.49)$$

$$RHS_{2,j} = \xi_{xi} (UP\ \omega_{i-1,j} - UM\ \omega^n_{i+1,j}) / \Delta\xi - \omega_y^n \xi_{xi} \Psi_{i-1,j} / \Delta\xi + \Psi_y^n \omega_x^n - \Psi_x^n \omega_y^n \quad (3.50)$$

Eqns (3.1) and (3.2) are solved using a special form of the Thomas algorithm for two partial differential equations. This algorithm, which is described in Appendix A, generates the solution to a block 2x2 set of equations in terms of recurrence coefficients. For the viscous region, the solution will have the form

$$\Psi_j = R_{1j} \Psi_{i,j+1} + S_{1j} \omega_{i,j+1} + T_{1j} \quad (3.51)$$

$$\omega_j = R_{2j} \Psi_{i,j+1} + S_{2j} \omega_{i,j+1} + T_{2j} \quad (3.52)$$

The terms R_{1j} ... T_{2j} are the recurrence coefficients. Boundary conditions are written in the form of Eqns (3.51) and (3.52) to find the recurrence. With the recurrence known at a boundary, the block tridiagonal algorithm can generate the remaining recurrence coefficients. There are two ways of solving the problem. The first way uses the wall boundary conditions to generate the recurrence and the interface conditions to generate the solution from Eqns (3.51) and (3.52). The second way is to use the boundary conditions at the interface to generate the recurrence and use the wall conditions to generate the solution. Since the current coupling scheme finds the solution at the interface, the first approach is taken. The wall boundary conditions are given by Eqns (2.54) and (2.56). Since Ψ is zero at the wall and Ψ and ω at j=2 are non-zero, in general, it follows from Eqn (3.51) that

$$R_{11} = 0 \tag{3.53}$$

$$S_{11} = 0 \tag{3.54}$$

$$T_{11} = 0 \tag{3.55}$$

The other recurrence at the wall are found by expanding Eqn (2.56)

$$\omega|_{y=0} = -\Psi_{yy}|_{y=0}$$

into the form of Eqn (3.52) and comparing the coefficients of Ψ and ω.

The resulting recurrence are

$$R_{22} = -(Q_{31} + Q_{11}) / \omega^* \quad (3.56)$$

$$S_{22} = 0 \quad (3.57)$$

$$T_{22} = 0 \quad (3.58)$$

With the recurrence known at the wall, the block tridiagonal solver can generate the remaining recurrence, where each block is a 2x2 matrix. Eqns (3.51) and (3.52) are then used to find the solution from the boundary condition at the interface.

Method II

Solution Procedure. The governing equations for this method are Eqns (2.37) and (2.39) in the viscous region and Laplace's equation (2.21) in the inviscid region. The inviscid solver is similar to the inviscid solver of method I with one exception. The lower boundary for this method takes the shape of the displacement thickness δ^* as shown in Figure 7. The inviscid solver now solves for flow over a displaced body where $\Psi = 0$. The remaining boundary conditions are unchanged. A shear transformation is applied to Laplace's equation to allow for a uniform grid in the computational domain. The solution procedures is as follows:

1) Assume an initial δ^*. Solve the inviscid region using the SLOR algorithm.

2) Evaluate U_e and V_e along the displaced body from the inviscid solution.

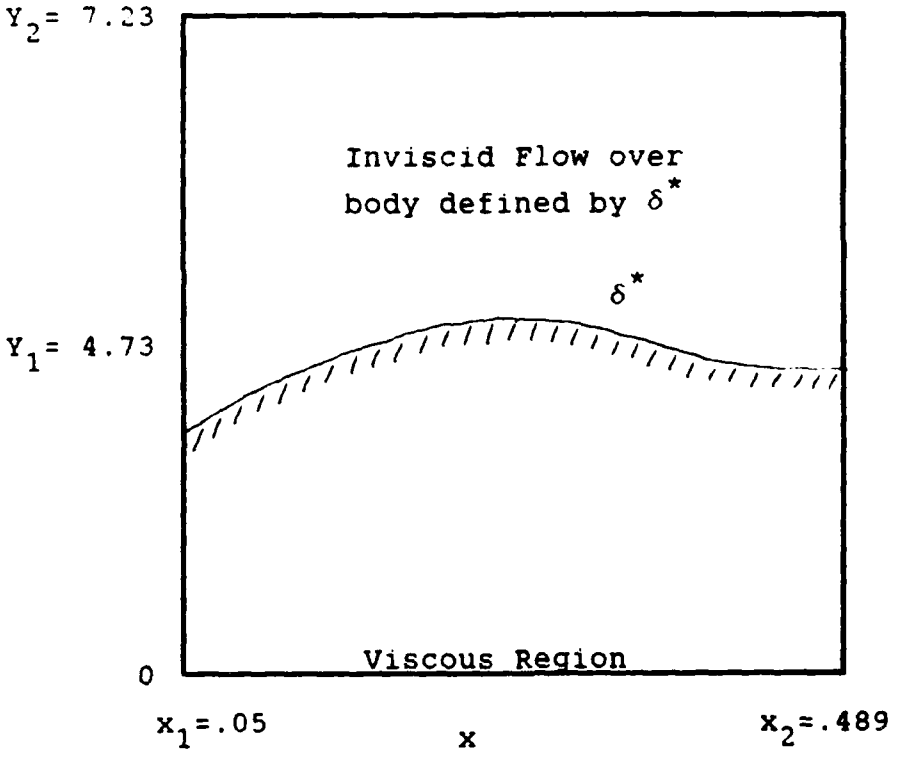

Figure 7. Flow geometry for Method II

3) Use a Runge-Kutta method [20] to solve for δ and C_f in Eqn (2.37) and Eqn (2.39), repeated here as

$$d/dx\left[U_e^2 \theta \right] + U_e \, (dU_e/dx) \, \delta^* = U_e^2 \, C_f/2$$

$$V_e = d/dx \left[U_e \, \delta^* \right] - \delta \, dU_e/dx$$

The momentum thickness θ, and the displacement thickness δ^* are written in terms of δ and C_f from Eqns (2.32) and (2.33) assuming a streamwise velocity profile based on the shear stress at the wall. This results in two equations and two unknowns. Note that U_e, V_e and dU_e/dx are known from Step 2.

4) Repeat steps (1) through (3) until δ^* does not change.

Inviscid Region. The model for the inviscid region is

$$\Psi_{xx} + \Psi_{yy} = 0$$

A shear transformation given by

$$\xi = x \tag{3.59}$$

$$\eta = y - \delta^* \, / \, H(x) \tag{3.60}$$

$$H(x) = y_e - \delta^* \tag{3.61}$$

is applied to allow for a uniform grid in the computational domain. The transformed Laplace equation becomes

$$\Psi_{\xi\xi} + \alpha \, \Psi_{\xi\eta} + \beta \, \Psi_{\eta\eta} + \zeta \, \Psi_{\eta} = 0 \tag{3.62}$$

where

$$\alpha = 2 \, H_x \, (\, 1 - \eta \,) \, / \, H \tag{3.63}$$

$$\beta = \left[H_x^2 \, (\, 1 - \eta^2 \,) + 1 \right] \, / \, H^2 \tag{3.64}$$

$$\zeta = (\, 1 - \eta \,) \, (\, H \, H_{xx} - 2 \, H_x^2 \,) \, / \, H^2 \tag{3.65}$$

Finite difference forms of the derivatives in Eqn (3.62) are given as

$$\Psi_{\xi\xi} = (\Psi_{i+1,j} - 2 \Psi_{i,j} + \Psi_{i-1,j}) / \Delta\xi^2 \qquad (3.66)$$

$$\Psi_{\xi\eta} = (3 \Psi_{i,j+1} - 4 \Psi_{i-1,j+1} + \Psi_{i-2,j+1}) / 4 \Delta\eta \Delta\xi - (3 \Psi_{i,j-1} - 4 \Psi_{i-1,j-1} + \Psi_{i-2,j-1}) / 4 \Delta\eta \Delta\xi \qquad (3.67)$$

$$\Psi_{\eta\eta} = (\Psi_{i,j+1} - 2 \Psi_{i,j} + \Psi_{i,j-1}) / \Delta\eta^2 \qquad (3.68)$$

$$\Psi_{\eta} = (\Psi_{i,j+1} - \Psi_{i,j-1}) / 2 \Delta\eta \qquad (3.69)$$

where a three point backward difference scheme is used for $\Psi_{\xi\eta}$ when $i > 2$. A two point backward difference scheme is used at i=2. Substituting Eqns (3.66)-(3.69) into Eqn (3.62) and rearranging gives

$$A_4^* \Psi_{i,j-1} + B_4^* \Psi_{i,j} + C_4^* \Psi_{i,j+1} = RHS_4^* \qquad (3.70)$$

where

$$A_4^* = \frac{-3 \alpha}{4 \Delta\eta \Delta\xi} + \frac{\beta}{\Delta\eta^2} - \frac{\zeta}{2 \Delta\eta} \qquad (3.71)$$

$$B_4^* = \frac{-2}{\Delta\xi^2} - \frac{2 \beta}{\Delta\eta^2} \qquad (3.72)$$

$$C_4^* = \frac{3 \alpha}{4 \Delta\eta \Delta\xi} + \frac{\beta}{\Delta\eta^2} + \frac{\zeta}{2 \Delta\eta} \qquad (3.73)$$

$$RHS_4^* = (-\Psi_{i+1,j}^{n})/\Delta\xi^2 - \Psi_{i-1,j}/\Delta\xi^2 + \alpha \Psi_{i-1,j+1}/\Delta\eta\Delta\xi - \alpha \Psi_{i-2,j+1}/4\Delta\eta\Delta\xi - \alpha \Psi_{i-1,j-1}/\Delta\eta\Delta\xi + \alpha \Psi_{i-2,j-1}/4\Delta\eta\Delta\xi \qquad (3.74)$$

A similar form of the equations are obtained for the case of i=2.

Relaxation is now added in the same manner as the finite difference inviscid solver. Solve for $\Psi_{i,j}$ in Eqn (3.70) and substitute into the right hand side of the relaxation relation

$$\Psi_{i,j} = (1 - W) \Psi_{i,j}^{n} + W \Psi_{i,j} \tag{3.75}$$

to obtain

$$A_4 \Psi_{i,j-1} + B_4 \Psi_{i,j} + C_4 \Psi_{i,j+1} = RHS_4 \tag{3.76}$$

where

$$A_4 = W A_4^* / B_4^* \tag{3.77}$$

$$B_4 = 1 \tag{3.78}$$

$$C_4 = W C_4^* / B_4^* \tag{3.79}$$

$$RHS_4 = (W RHS_4^* / B_4^*) + (1 - W) \Psi_{i,j}^{n} \tag{3.80}$$

Boundary conditions are now applied to find the values of $A_4 \ldots RHS_4$ for the special cases of j=2 and j=JMAX-1. At j=2, $\Psi = 0$, and therefore

$$A_4|_{j=2} = 0 \tag{3.81}$$

At the outer boundary the conditions are given by Howarth's velocity profile, rewritten as

$$\Psi_y|_{j=JMAX} = PY(I) \tag{3.82}$$

Equation (3.82) written in finite difference form in the computational domain yields

$$\Psi_{i,JMAX} = \Psi_{i,JMAX-1} + H \, PY(I) \, \Delta\eta \tag{3.83}$$

Equation (3.76) written at j=JMAX-1 is simply

$$A_4 \Psi_{i,JMAX-2} + B_4 \Psi_{i,JMAX-1} + C_4 \Psi_{i,JMAX} = RHS_4 \tag{3.84}$$

Substituting Eqn (3.83) into Eqn (3.84) and rearranging gives the coefficients $A_4 \ldots RHS_4$ at j=JMAX-1 as

$$RHS_4 = RHS_4 - C_4 \; PY(I) \; H \; \Delta\eta \tag{3.85}$$

$$B_4 = B_4 + C_4 \tag{3.86}$$

$$C_4 = 0 \tag{3.87}$$

where the order of these calculations must be honored. With all the coefficients known, the system solver used in the other inviscid solver can be used. The solution procedure is identical at this point to the previous inviscid algorithm.

Viscous Region. The solution to the IBL equations (2.37) and (2.39) start by assuming a streamwise velocity profile written in terms of the wall shear stress. The general form is given by

$$u = AU + BU\, y + CU\, y^2 + DU\, y^3 + EU\, y^4 + FU\, y^5 \tag{3.88}$$

where AU-FU are determined by the boundary conditions

$$(1)\; u_{|y=0} = 0$$

$$(2)\; u_{|y=\delta} = U_e$$

$$(3)\; u_{y|y=\delta} = 0$$

$$(4)\; u_{yy|y=\delta} = 0$$

$$(5)\; u_{y|y=0} = \tau_w/\mu$$

$$(6)\; u_{yyy|y=0} = 0 \tag{3.89}$$

A fifth degree polynomial was chosen after it was found that a fourth degree form did not provide adequate accuracy.

Imposing Eqn (3.89) on Eqn (3.88) results in

$$AU = 0$$

$$BU = \tau_w/\mu$$

$$CU = (10/3)\ U_e\ \delta^{-2} - 2(\tau_w/\mu)\ \delta^{-1}$$

$$DU = 0$$

$$EU = 2(\tau_w/\mu)\ \delta^{-3} - 5\ U_e\ \delta^{-4}$$

$$FU = (8/3)\ U_e\ \delta^{-5} - (\tau_w/\mu)\ \delta^{-4} \qquad (3.90)$$

Eqn (3.90) can be put in non-dimensional form using Eqn (2.35), rewritten here as

$$C_f = 2\tau_w/\rho u_x^2$$

and by considering the non-dimensional forms given in Eqn (3.4). Eqn (3.90) in non-dimensional form is therefore

$$AU = 0$$

$$BU = R_e\ C_f/2$$

$$CU = (10/3)\ U_e\ \delta^{-2} - R_e\ C_f\ \delta^{-1}$$

$$DU = 0$$

$$EU = R_e\ C_f\ \delta^{-3} - 5\ U_e\ \delta^{-4}$$

$$FU = (8/3)\ U_e\ \delta^{-5} - (R_e/2)\ C_f\ \delta^{-4} \qquad (3.91)$$

Eqn (3.91) substituted into Eqn (3.88) defines the non-dimensional form of the streamwise velocity u. Eqn (3.88) can now be substituted into Eqns (2.32) and (2.33) to obtain expressions for the momentum and displacement thicknesses in terms of C_f and δ.

While these calculations for C_f and δ are straightforward, they are also very long and tedious for the case of finding the momentum thickness θ (See Appendix C). The results are given as

$$\delta^* = A\,\delta - B\,C_f\,\delta^2\,U_e^{-1} \tag{3.92}$$

where,

$$A = 4/9 \tag{3.93}$$

$$B = R_e/30 \tag{3.94}$$

and

$$\theta = C\,\delta + D\,C_f\,\delta^2\,U_e^{-1} - E\,C_f^2\,\delta^3\,U_e^{-2} \tag{3.95}$$

where,

$$C = 0.115440115 \tag{3.96}$$

$$D = 8.297258e\text{-}03\ R_e \tag{3.97}$$

$$E = 1.695526e\text{-}03\ R_e^2 \tag{3.98}$$

Eqns (3.92) and (3.95) can now be substituted into the IBL equations

$$d/dx\left[\,U_e^2\theta\,\right] + U_e\,(dU_e/dx)\,\delta^* = U_e^2\,C_f/2 \tag{2.37}$$

$$V_e = d/dx\,\left[\,U_e\,\delta^*\,\right] - \delta\,dU_e/dx \tag{2.39}$$

to obtain two equations in two unknowns, δ and C_f. Once the equations are solved, δ^* can be found from Eqn (3.92) to obtain the new shape of the displaced body for the next cycle of the inviscid solver discussed in the previous section.

Two methods for solving the IBL equations are Newton's method for finding roots of algebraic equations and the fourth order Runge-Kutta method for integrating first order, ordinary differential equations. Both were implemented for the IBL method, but only the Runge-Kutta method [20] was used in the final results. The IBL equations are written as

$$d\delta/dx = F_1(C_f,\delta) \tag{3.99}$$

$$d(C_f)/dx = F_2(C_f,\delta) \tag{3.100}$$

where F_1 and F_2 are functions of C_f and δ. The integration starts at $x_1 = .05$ and ends at $x_2 = .489$. The expressions for F_1 and F_2 will now be found. Eqn (2.37) written in terms of C_f and δ becomes

$$2U_eU_{ex}C\delta + CU_e^2\delta_x + DU_{ex}C_f\delta^2 + DU_e\delta^2C_{fx} + 2DU_eC_f\delta\delta_x$$
$$-2EC_f\delta^3C_{fx} - 3EC_f^2\delta^2\delta_x - U_e^2C_f/2 + U_eU_{ex}A\delta$$
$$- BU_{ex}C_f\delta^2 = 0 \tag{3.101}$$

While Eqn (2.39) becomes

$$V_e = A\delta_xU_e + A\delta U_{ex} - 2BC_f\delta\delta_x - B\delta^2C_{fx} - U_{ex}\delta \tag{3.102}$$

F_1 is found by solving for C_{fx} in Eqn (3.101) and substituting into Eqn (3.102). This results in an equation of the form of Eqn (3.99), where

$$F_1(C_f,\delta) = \Big[-A\delta U_{ex} - 2BC\delta^3U_eU_{ex}z^{-1} - BDC_f\delta^4U_{ex}z^{-1}$$
$$+(1/2)BC_f\delta^2U_e^2z^{-1} - ABU_e\delta^3U_{ex}z^{-1} + B^2C_f\delta^4U_{ex}z^{-1}$$
$$+U_{ex}\delta + V_e \Big] / K \tag{3.103}$$

and,

$$z = D\,U_e\,\delta^2 - 2\,E\,C_f\,\delta^3 \tag{3.104}$$

$$K = AU_e - 2BC_f\delta + BC\delta^2U_e{}^2z^{-1} + 2BDC_f\delta^3U_ez^{-1} - 3BEC_f{}^2\delta^4z^{-1} \tag{3.105}$$

$F_2(C_f,\delta)$ is found by solving for δ_x in Eqn (3.102) and substituting into Eqn (3.101). The result is

$$F_2(C_f,\delta) = \Big[-2U_eU_{ex}C\delta - CU_e{}^2Q - DU_{ex}C_f\delta^2 - 2DU_eC_f\delta Q + 3EC_f{}^2\delta^2Q + U_e{}^2C_f/2 - A\delta U_eU_{ex} + BU_{ex}\,C_f\,\delta^2 \Big] / M \tag{3.106}$$

where,

$$P = A\,U_e - 2\,B\,C_f\,\delta \tag{3.107}$$

$$Q = P^{-1}\,(\,V_e - A\,\delta\,U_{ex} + \delta\,U_{ex}\,) \tag{3.108}$$

$$M = P^{-1}\,(\,CU_e{}^2B\delta^2 + 2BDU_eC_f\delta^3 - 3EBC_f{}^2\delta^4\,) + DU_e\delta^2 - 2EC_f\delta^3 \tag{3.109}$$

With F_1 and F_2 determined, Eqns (3.99) and (3.100) are solved using a fourth order Runge-Kutta algorithm. The solution produces C_f and δ for each streamwise location. The displacement thickness δ^* is calculated and used as the input to the inviscid solver, which produces a new U_e, U_{ex} and V_e from the inviscid solution. This cycle continues until the convergence criteria on δ^* is satisfied.

Method III

This method solves the Boundary Layer (BL) equations in the viscous region and uses the Hilbert Integral, Eqn (2.47), to obtain the viscous correction to the inviscid velocity. The ANS equations used in the finite difference method are reduced to the BL equations by setting $\Psi_{xx} = 0$. The solution procedure is as follows:

(1) Assume the displaced body defined by $\delta^*(x)$.

(2) Solve the BL equations by solving Eqn (2.19) and (2.20) with $\Psi_{xx} = 0$. The boundary condition at the outer boundary is known from prescribing δ^* in (1). Calculate $U_{e,bl}$, the streamwise velocity at the BL edge.

(3) Solve the Hilbert integral

$$\delta u = \pi^{-1} \int_{x_1}^{x_2} \left[d(U_e \delta^*)/d\xi \right] (x-\xi)/r^2 \; d\xi \qquad (2.47)$$

using trapezoidal integration. On the first pass U_e in Eqn (2.47) is set to Howarth's velocity, PY. On later passes U_e is taken as the current value, which will be denoted as $U_{e,h}$. Calculate the inviscid BL velocity $U_{e,h}$ as

$$U_{e,h} = PY + \delta u \qquad (3.110)$$

(4) Generate a new $\delta^*(x)$ based on $U_{e,bl}$ and $U_{e,h}$ using the following relation

$$\delta^{*\,n+1} = \delta^{*\,n} \left(U_{e,bl} / U_{e,h} \right) \qquad (3.111)$$

This simple method for updating δ^* was used by Carter and is described in Reference [1]. It was noticed that small deviations in the local U_e tends to preserve the volume flow rate per unit width in the BL. Therefore, $U_e\ \delta^* \cong$ constant. A local decrease in U_e (adverse pressure gradient) causes an increase in δ^* and vice versa. Adding over-relaxation to Eqn (3.111) results in

$$\delta^{*\,n+1} = \delta^{*\,n}\left[1 + W\left(\left(U_{e,bl}/U_{e,h}\right) - 1\right)\right] \qquad (3.112)$$

(5) With a new δ^*, repeat (2)-(3) until $U_{e,bl} = U_{e,h}$ within a set tolerance level.

IV Results and Discussion

The three methods discussed in Chapter 3 were applied to Howarth's flow over a flat plate. The flow is incompressible with a Reynolds number of R_e=20800. Results are given and comparisons made where applicable. Discussion on the significant aspects of each method are also given.

Method I

The flow geometry for this method was shown in Figure 2 of Chapter 2. Briley [16] solved this problem with an Alternating-Direction-Implicit (ADI) scheme using the full Navier-Stokes equations. The fundamental difference between Briley's approach and the current approach is the treatment of the solution domain. Briley solved the Navier-Stokes equations within a single region where no distinction is made between inviscid and viscous flows. The current solver breaks up the solution domain into a viscous region and an inviscid region that are implicitly coupled together. The advantage of the current method is clear if the inviscid region is much larger than the viscous region. For this case, the relatively simple inviscid model is solved over most of the domain while the ANS equations are solved over a small region of that domain. Using the full Navier-Stokes equations in such a domain would be quite expensive in terms of computation time. However, Briley selected an outer boundary that is very close to the edge of the boundary

layer. Therefore, a comparison of computation times between these two methods will not demonstrate the utility of the current method. It can be said, however, that the larger the inviscid region, the greater the amount of computational savings using the current method versus using the Navier-Stokes equations in a single solution domain.

Briley's work was used as a checkcase for the current finite difference method. The displacement thickness δ^* from Briley was prescribed at the edge of the current viscous solver. The resulting coefficient of friction compared very well to Briley's C_f as shown in Figure 8. The grids used for this comparison were (35x30) for Briley and (151x74) for the current viscous solver. The comparison shows that the viscous solver is working properly. The entire current method was then run for the case of a coarse (30x35) grid used by Briley, an intermediate (76x74) grid, and a fine (151x74) grid. The inviscid grid was the same as the viscous grid in the number of x points with 4 grid points used in the y direction. All the grids were uniform. The resulting C_f and δ^* are shown in Figures 9 and 10 respectively. The difference in the separation region is due to the treatment of the boundary conditions. With the current zonal technique the boundary conditions are not imposed the same way as in Briley's case.

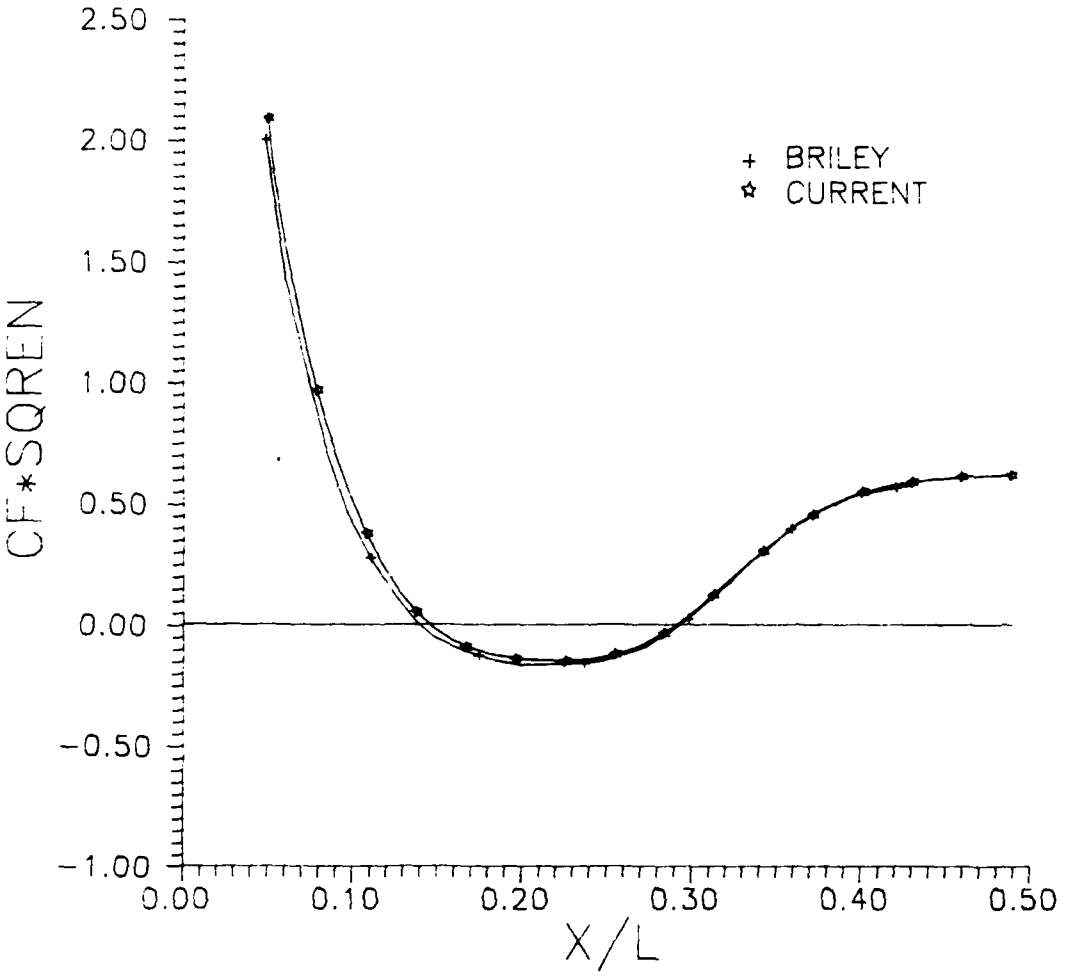

Figure 8. Skin friction coefficient comparison between current viscous solver and Briley

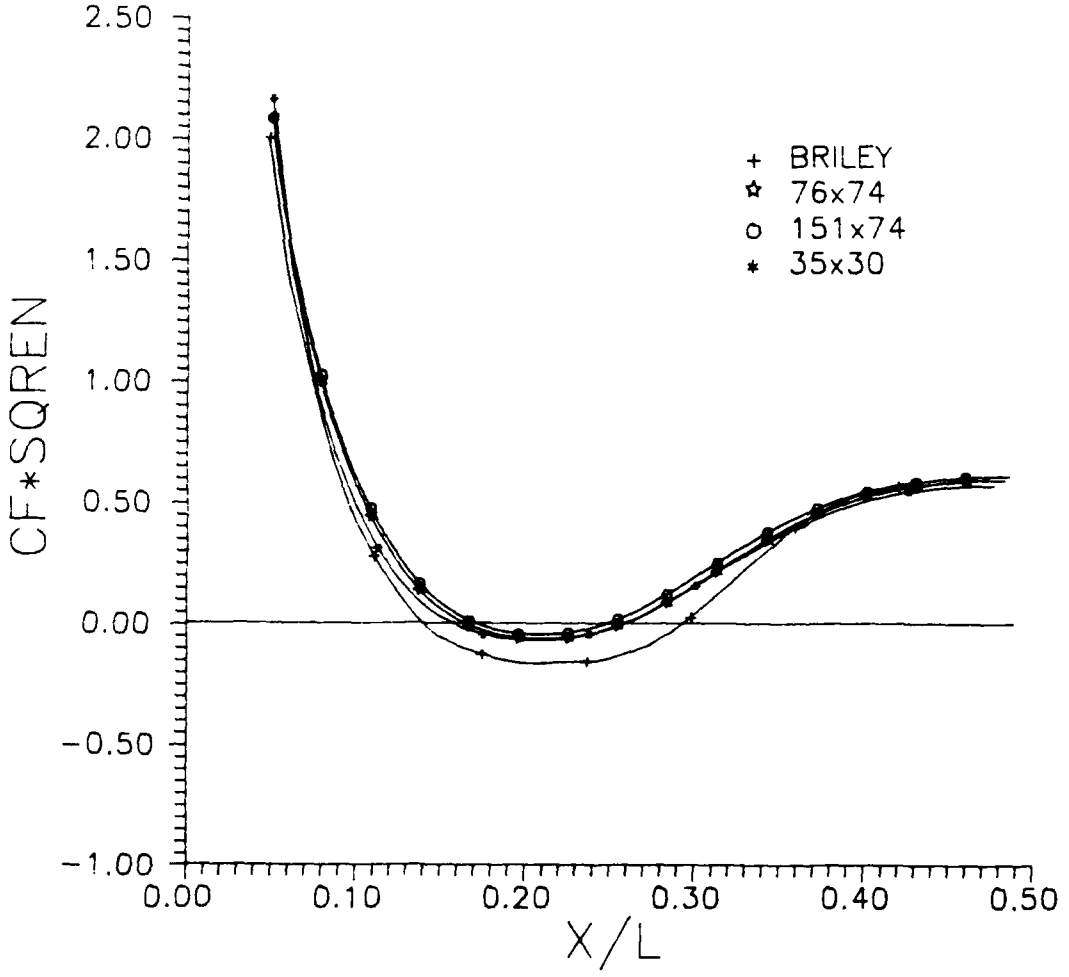

Figure 9. Skin friction coefficient for various grids

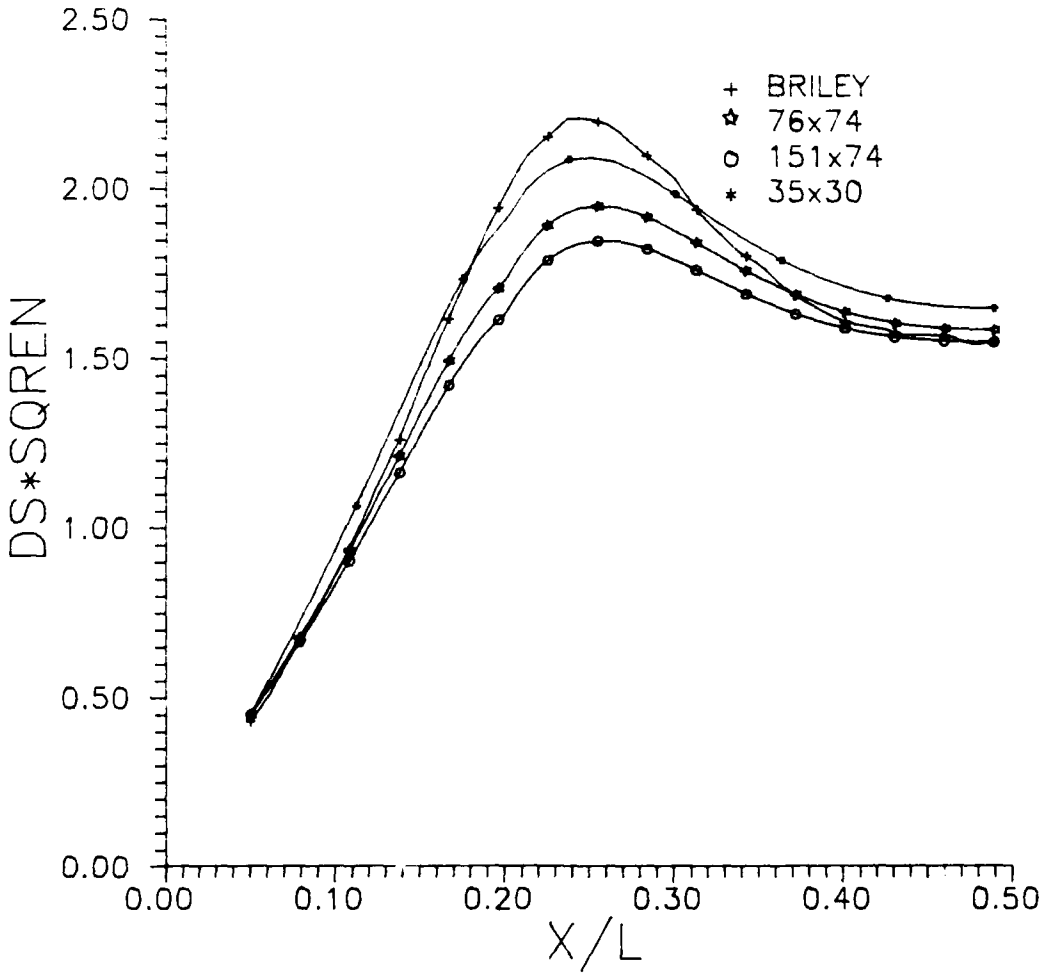

Figure 10. Displacement thickness for various grids

Briley [16] prescribed zero vorticity and Howarth's velocity at the outer edge of his solution domain. In Method I, the condition of zero vorticity is imposed at the edge of the boundary layer and Howarth's velocity condition is imposed at the outer boundary of the inviscid region. It is this distinction in the boundary conditions that accounts for the difference in the two solutions. When prescribing δ^* at the edge of the viscous region, as was done for the case shown in Figure 8, the separation region grows as the grid is refined. However, as Figure 9 shows, the current method produces a smaller separation region as the grid is refined. This event is explained by examining Figure 10, which shows that refining the grid in the current method produces a lower δ^*. This results in a lower C_f as well. In Briley's case, however, the same δ^* is prescribed for each refinement of the grid. The two approaches are fundamentally different.

Streamline contours for the current method are shown in Figure 11 for the intermediate (76x74) grid. The x axis was scaled for plotting purposes only, and represents the plate for x_1=0.05 to x_2=0.489. The important result from Figure 11 is that the streamlines at the interface (Y=4.73) are completely continuous. The coupling scheme produces a smooth, continuous solution between the viscous and inviscid regions.

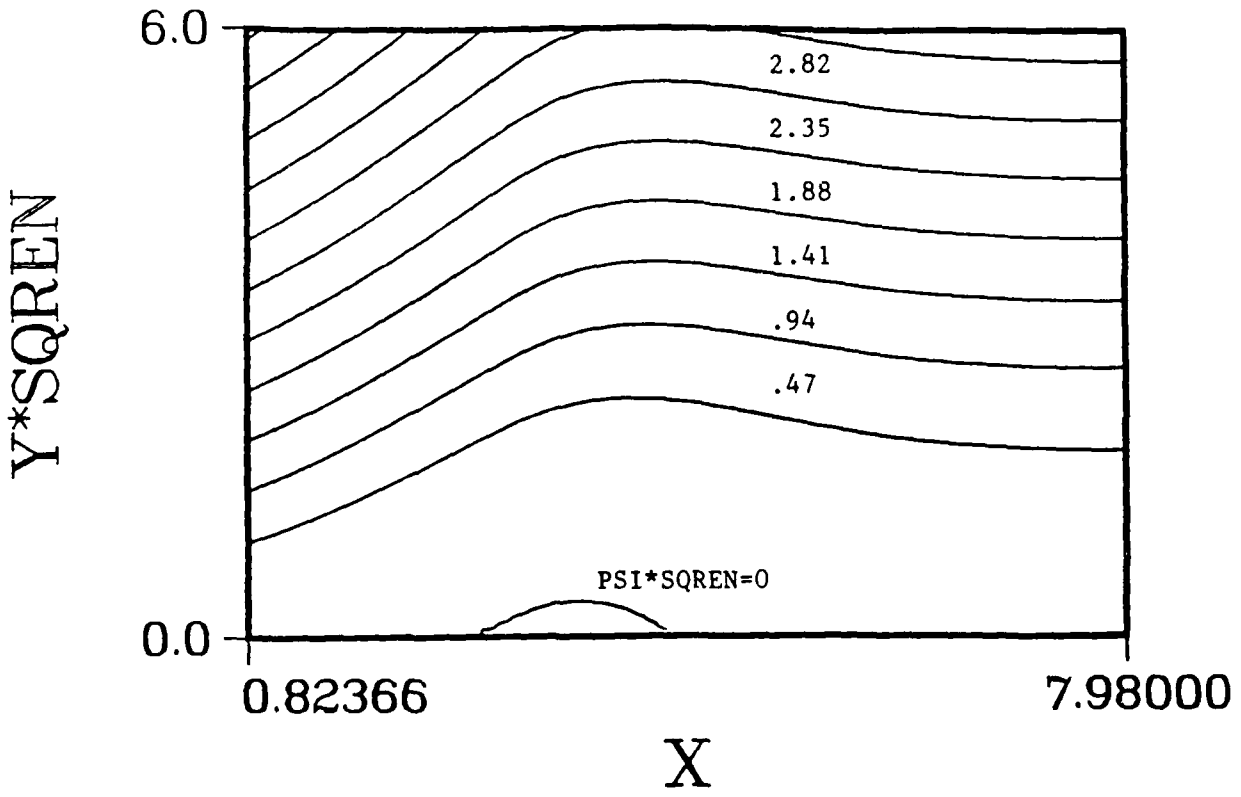

Figure 11. Streamline contours for Method I

Figure 12 compares the predicted inviscid velocity at the interface using Method I to Howarth's velocity. The difference in these two curves is due to viscous effects.

The current method was also run for a higher value of the corner velocity X_0, with the expectation that a higher X_0 will result in a longer region of adverse pressure, which should result in a larger separation region. This was exactly the case as shown in Figure 13. Here X_0 was increased from 0.2 to 0.21. The resulting increase in the separation region is apparent from the figure.

The computation times for the current method for the coarse, intermediate, and fine grids are 55, 579, and 4101 CPU seconds respectively on the ASD CYBER. The convergence history for the intermediate grid is shown in Figure 14. The residual tolerance was 10^{-5} for all grids. The approximate memory use is 14600 words for the intermediate grid.

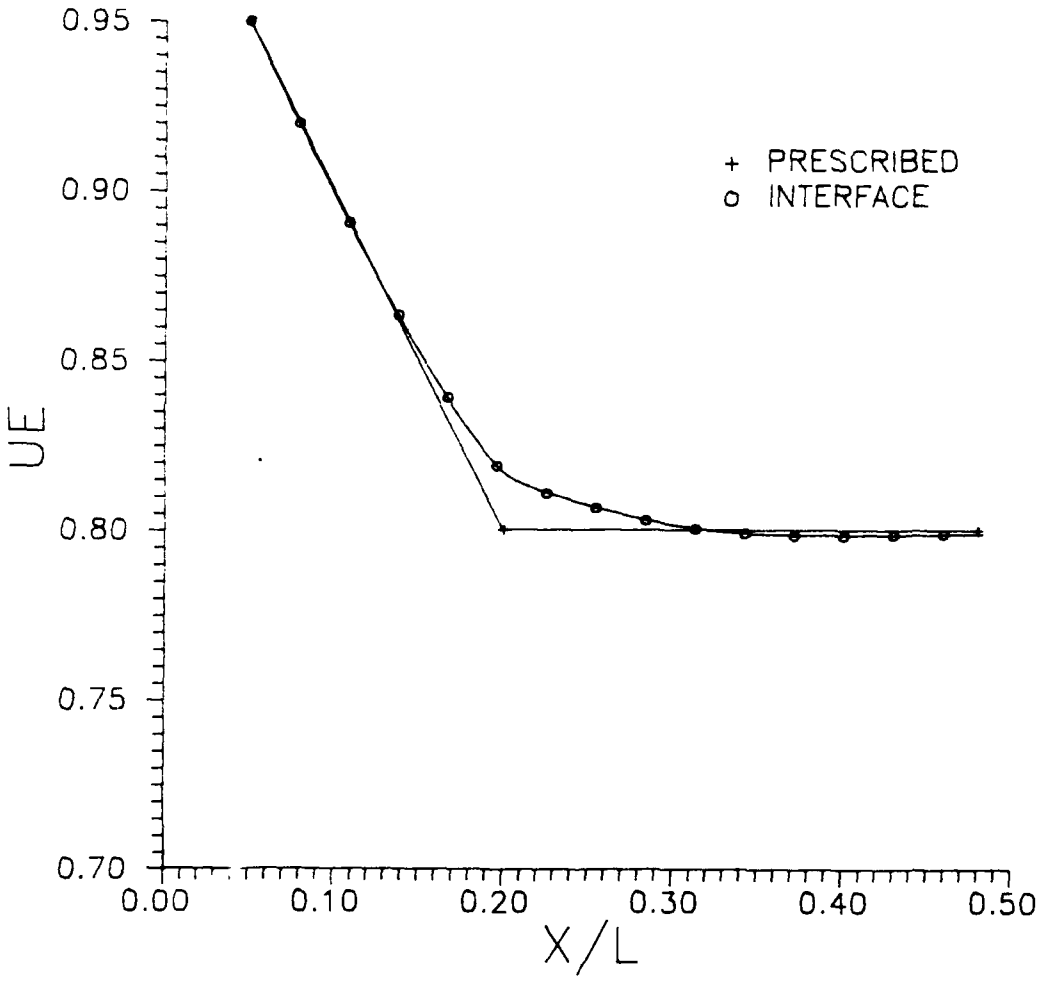

Figure 12. Prescribed velocity profile versus velocity at interface

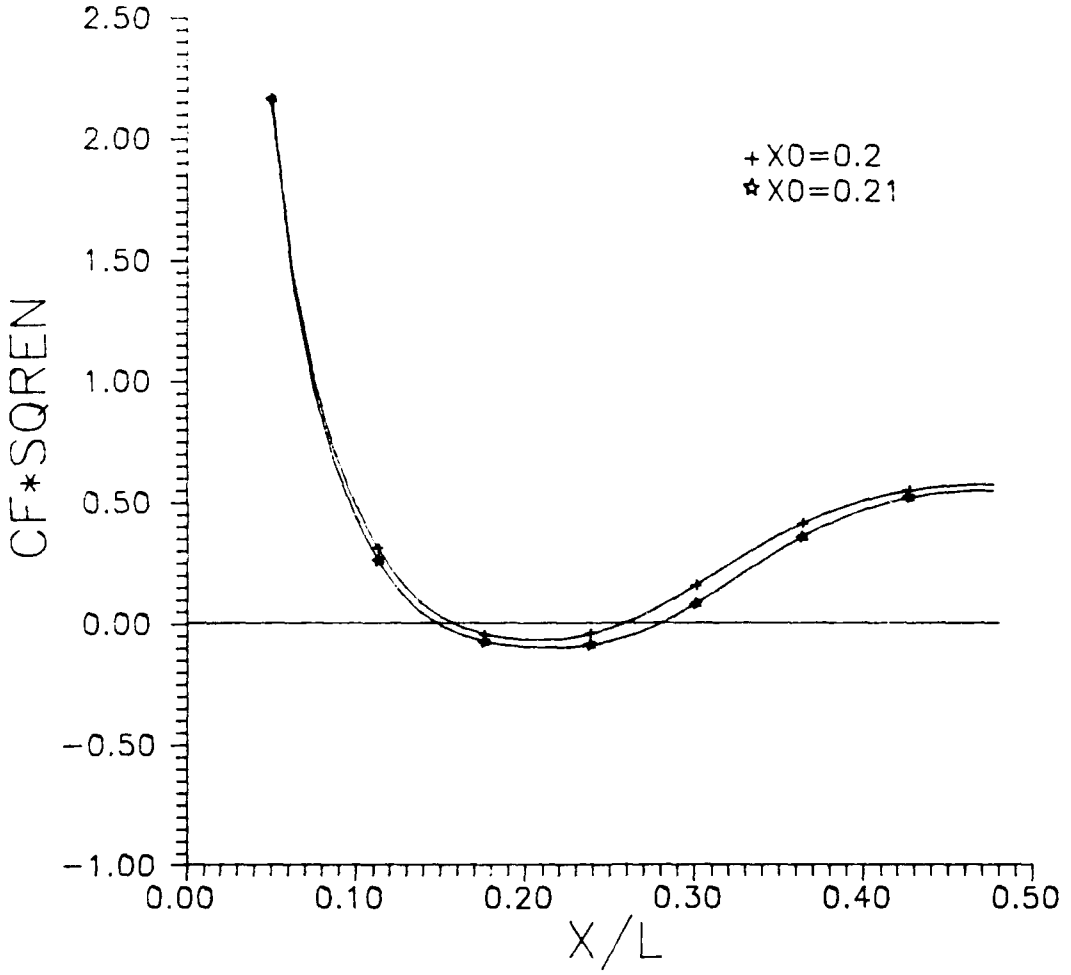

Figure 13. Skin friction comparison for different values of X_0

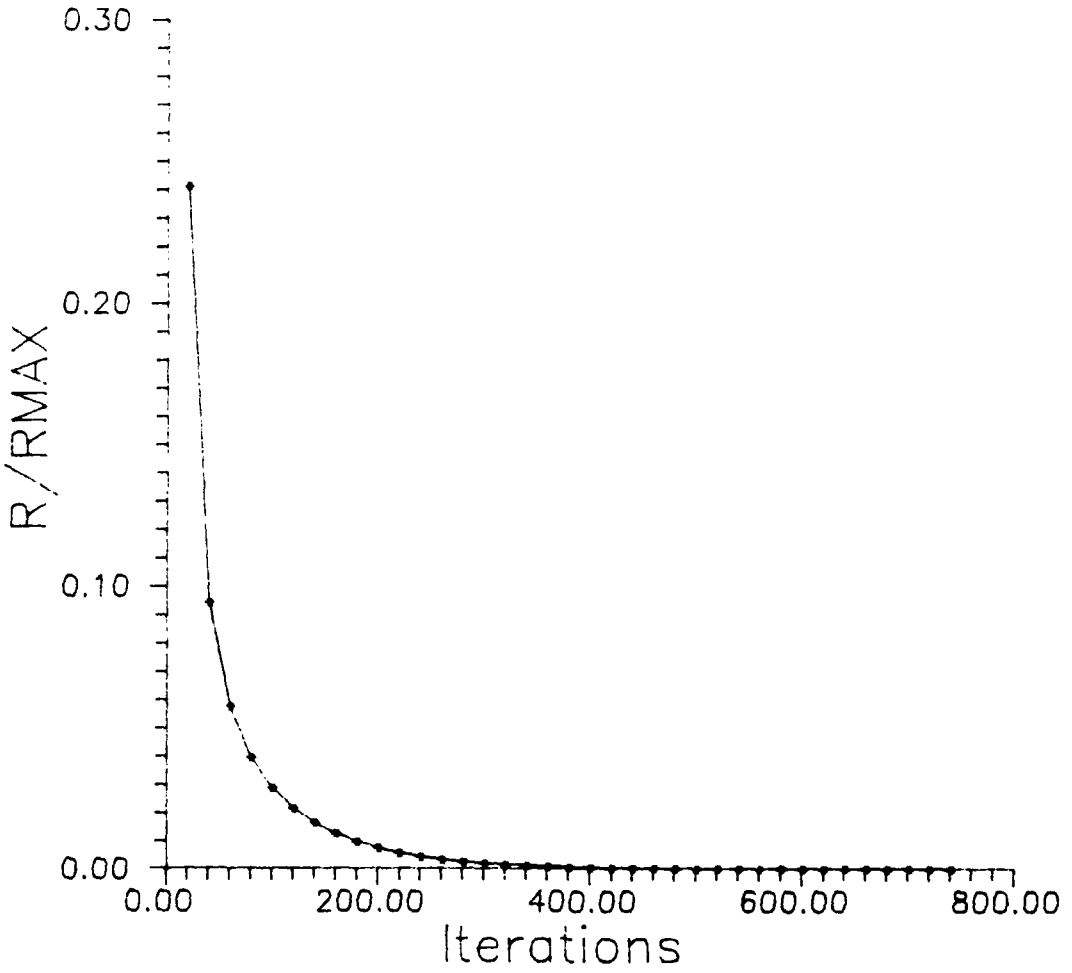

Figure 14. Convergence history for Method I

Method II

The IBL method was described in Chapter 3. The fifth degree velocity profile, along with the IBL equations, modeled the viscous region. The inviscid region solved the finite difference form of Laplace's equation for a non-uniform grid. The inviscid grid is (76x51), with the outer boundary at the same location as the finite difference method. The residual tolerance value is 10^{-6}. Relaxation was used in the inviscid region where W was finally chosen to be 1.3.

The IBL method was first executed with δ^* and U_e from the finite difference method used as the initial conditions. For this special case, the inviscid solver is not required since U_e is given. The normal velocity can be calculated knowing δ^* and U_e. The resulting C_f for only one iteration of the method is shown in Figure 15. The excellent agreement between this C_f and Briley's C_f demonstrates that the method can be a useful alternative to solving the viscous region. The CPU time required to solve the viscous region is 0.122 seconds on the ASD CYBER. In addition, Figure 15 shows that this rather simple method is clearly capable of solving for flows with an adverse pressure gradient; including flow separation. Further iterations of the current IBL algorithm results in an instability in the solution, which result in very inaccurate values of C_f past $x \cong 0.3$. The primary reason for this behavior is thought to be the assumption of the velocity profile.

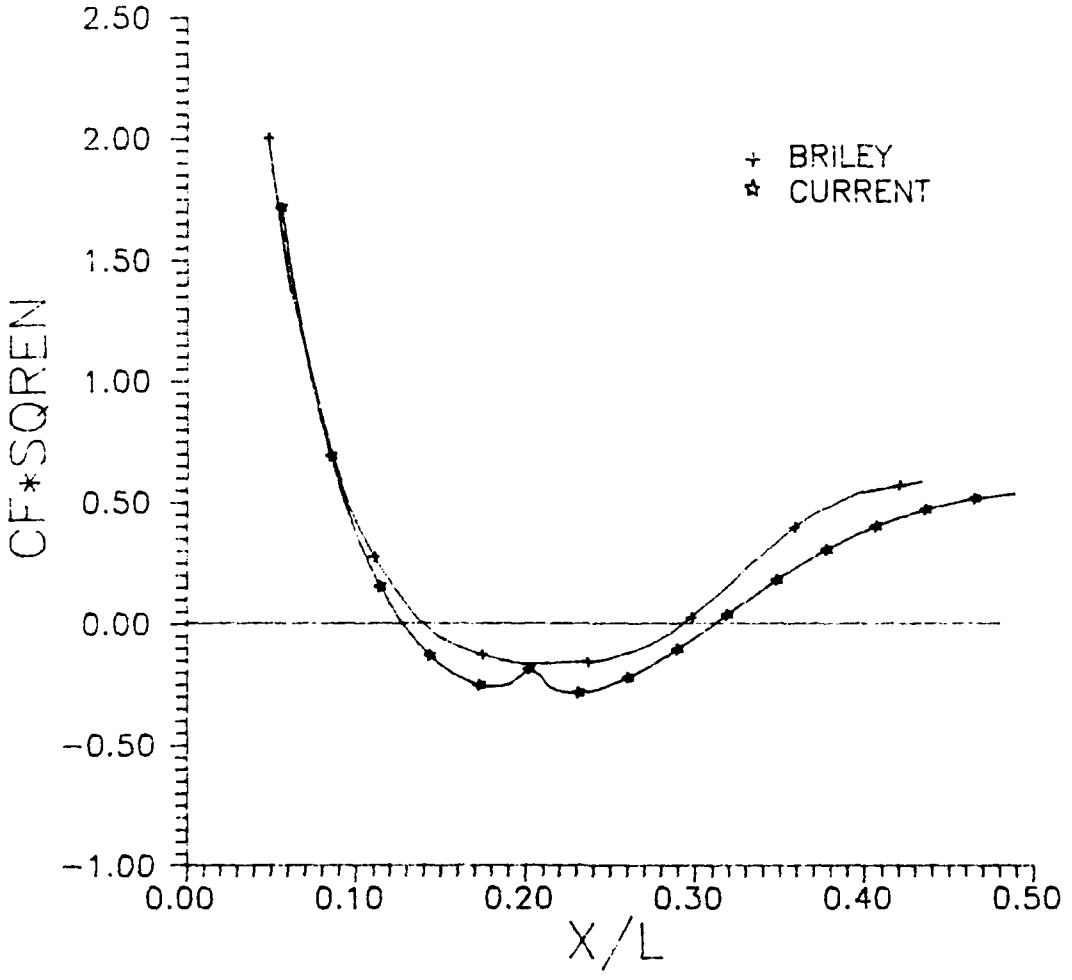

Figure 15. Skin friction for Method II

Figure 16 shows the resulting C_f for the case of a fourth degree and a fifth degree velocity profile with the same inputs of δ^* and U_e. Notice that the improvement in the solution between the two cases is due to the accuracy of the assumed velocity profile. The fourth degree profile was generated with the same boundary conditions as the fifth degree profile, except that $u_{yy}|_{y=\delta} \neq 0$ for the fourth degree profile. Further accuracy in the method should be attainable by specifying a sixth degree profile, where $u_{yyy}|_{y=\delta} = 0$ would provide the additional boundary condition.

An additional run with the IBL method was made to investigate the small ridge in the C_f of Figure 14 at x=0.2. This ridge is believed to be caused by a slight irregularity in the input δ^*. To confirm this hypothesis, a sixth degree polynomial was generated to have the approximate shape of the displacement thickness. This δ^* is shown in Figure 17. The U_e was obtained using the inviscid solver. The resulting C_f, shown in Figure 18, shows that smooth, continuous output is obtained from the method when a smooth δ^* is used as the input. This verifies that the small ridge in the C_f of Figure 15 is due to an irregularity in the displacement thickness. This is an important point, since the inviscid solver uses first and second derivatives of δ^* to obtain the transformation parameters of the computational grid.

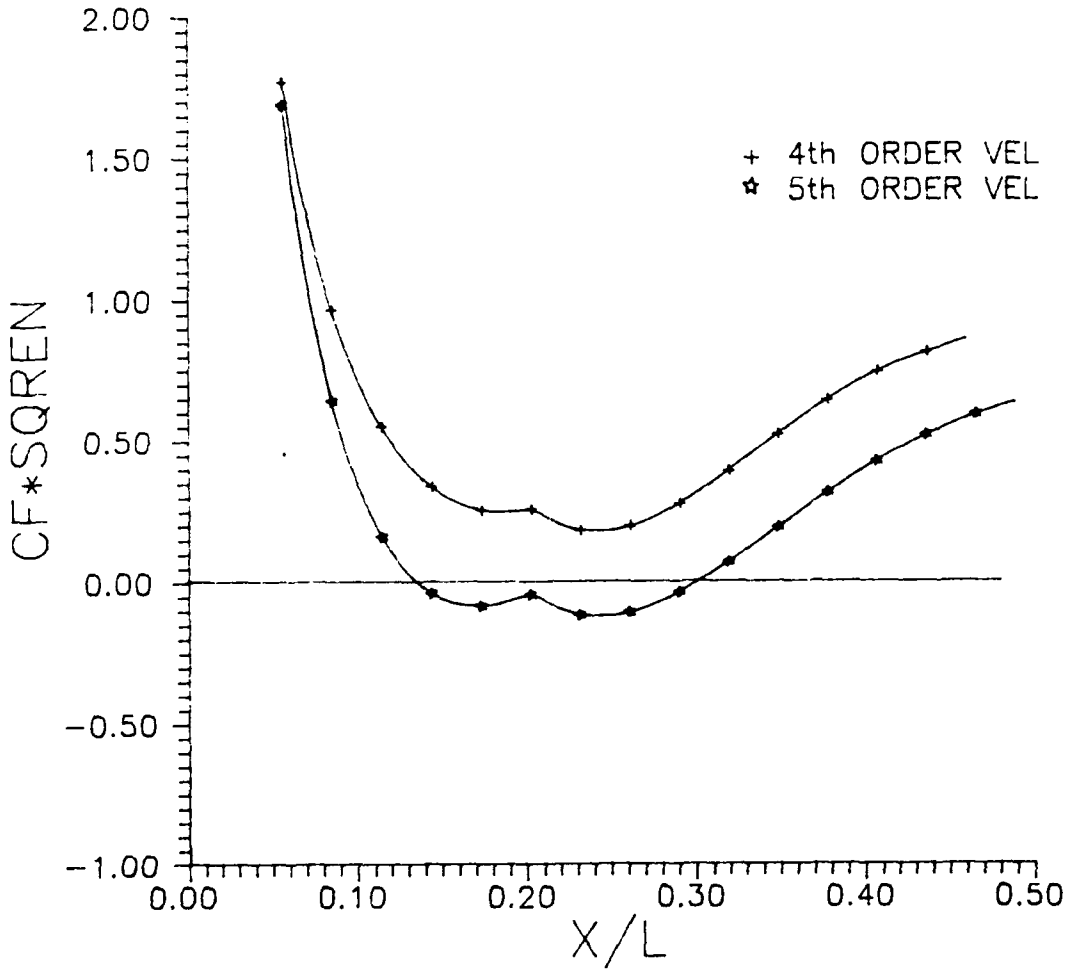

Figure 16. Skin friction comparison for fourth and fifth order velocity profiles

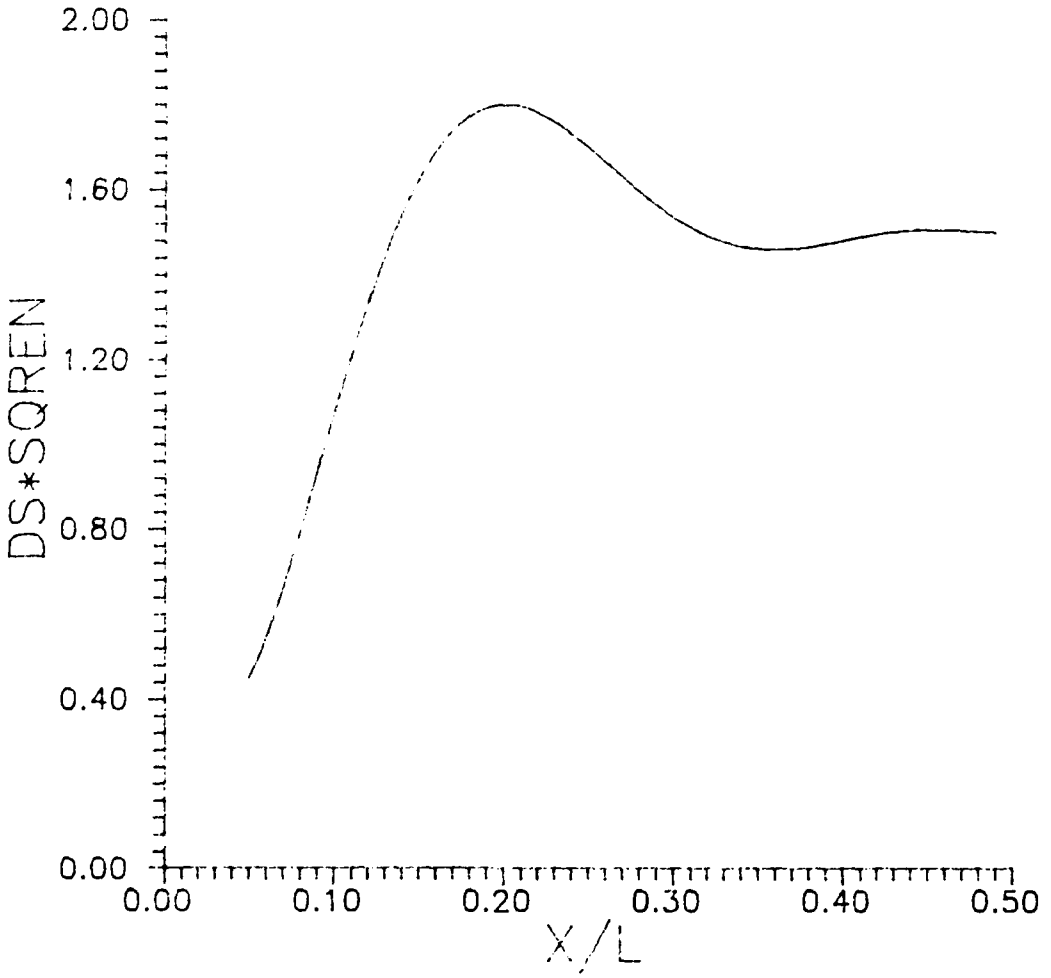

Figure 17. Polynomial displacement thickness

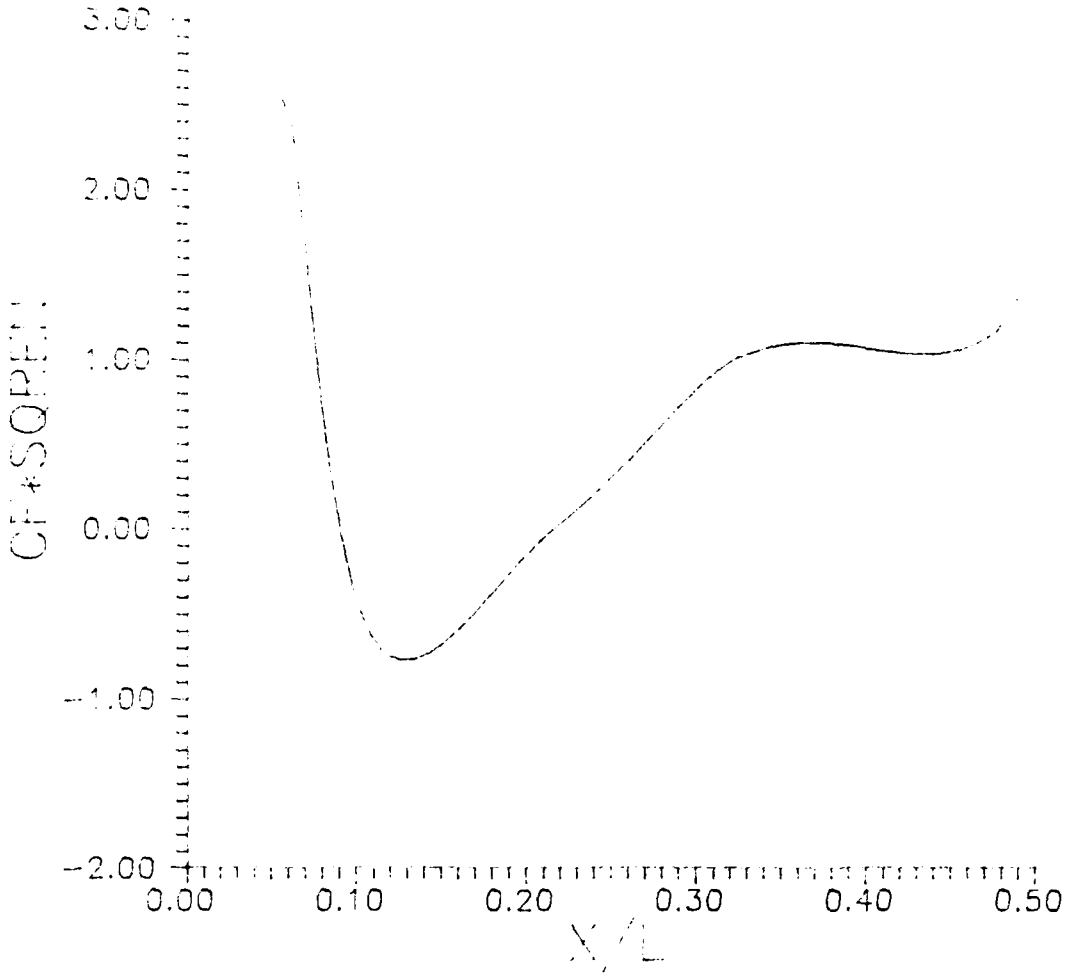

Figure 18. Skin friction for polynomial displacement thickness

The total CPU time for one cycle of the IBL method is 38.622 seconds, where 38.5 of this time is due to the inviscid solver and the calling program. This time can be greatly reduced by using less grid points, by reducing the residual tolerance to 10^{-5}, and possibly by using an ADI method. The memory requirements are approximately 17000 words, of which 11,628 words are used to store the transformation parameters α, β, and ζ over the (76x51) grid. These parameters are stored to calculate the residuals. A scheme could be developed to calculate the residuals locally in the flow by saving only three local columns of the data. This would reduce the total memory requirements down to approximately 5500 words.

Method III

Method III was explained in Chapter 3. The boundary layer equations are solved over the viscous region. The Hilbert Integral, Eqn (2.47), is then solved to obtain the correction to the inviscid velocity due to viscous effects. The method iterates until U_e from the boundary layer calculation matches U_e obtained from the Hilbert integral calculation. The resulting C_f for this method is shown in Figure 19 for two values of X_0. The data near the inlet at x_1 and at the corner position X_0 required smoothing due to a weak instability at these points.

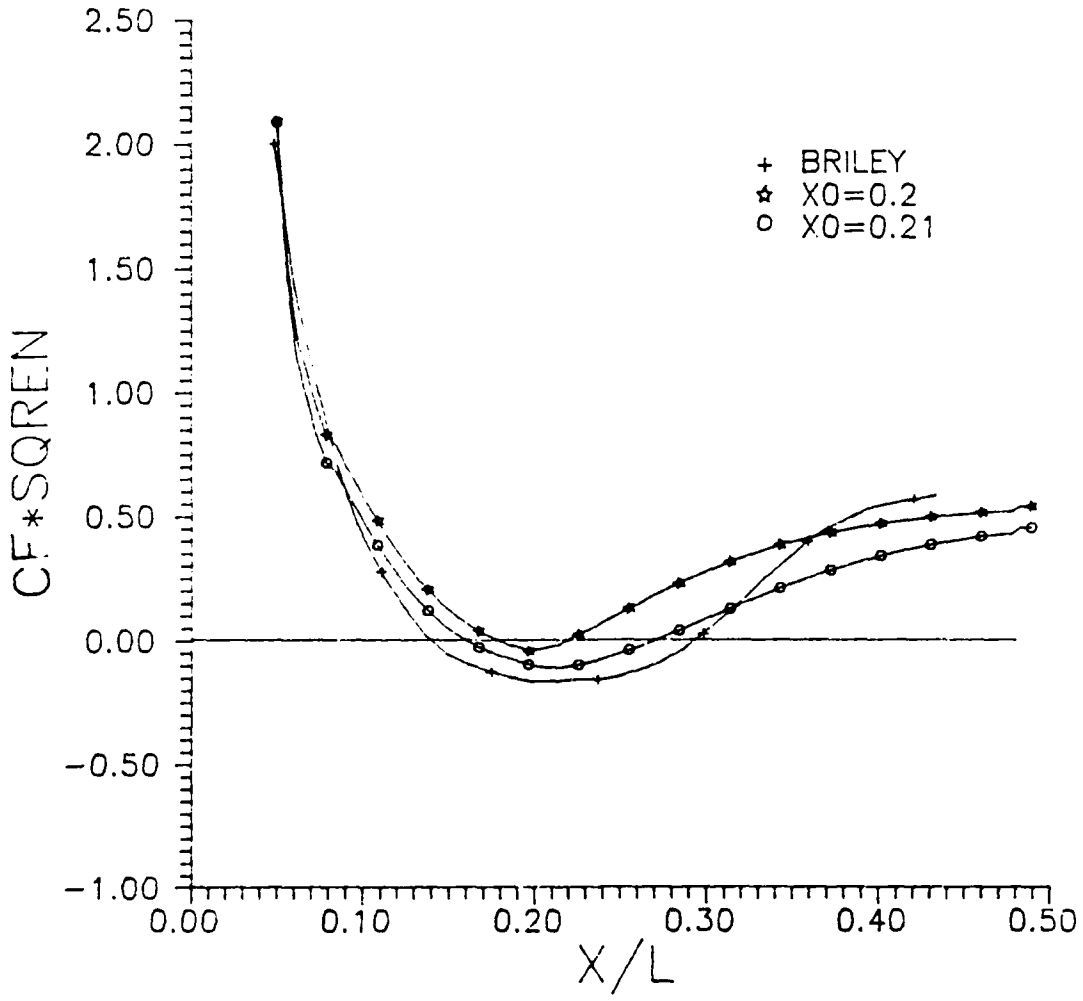

Figure 19. Skin friction for Method III

This instability was also noticed by Cebeci and Stewartson [21], who added several modifications to their algorithm to smooth the introduction of the Hilbert integral near the inlet. The most severe modification was the addition of an artificial correction term to the Hilbert integral that added a maximum δu at the inlet and added less δu as x increased. Cebeci also multiplied R_e by the term $\mathrm{cosec}((x-x_1)/2\Delta x)$ in the integration over the first four points to further smooth the data. The only modification to the current method was to smooth the data near the inlet and near the corner position X_0. Adding an artificial term to δu may help smooth the resulting data, however it also directly adds an error to the solution. Indeed, Cebeci's result for C_f showed no separation at all for the case of $X_0 = 0.21$. Figure 19 clearly shows separation for this case and is in excellent qualitative agreement with Briley's result. The slight irregularity of the solution in Figure 19 near the inlet is of little concern. Additional smoothing can be done but it will not affect the overall trends in the solution. The displacement thicknesses for the current method are shown in Figure 20. They are in qualitative agreement with the δ^* from the finite difference method and from Briley's results. The resulting boundary layer edge velocities are shown in Figure 21. UEBL is U_e from the boundary layer analysis and UEH is from the Hilbert integral calculation. As expected, the two profiles match for the converged solution.

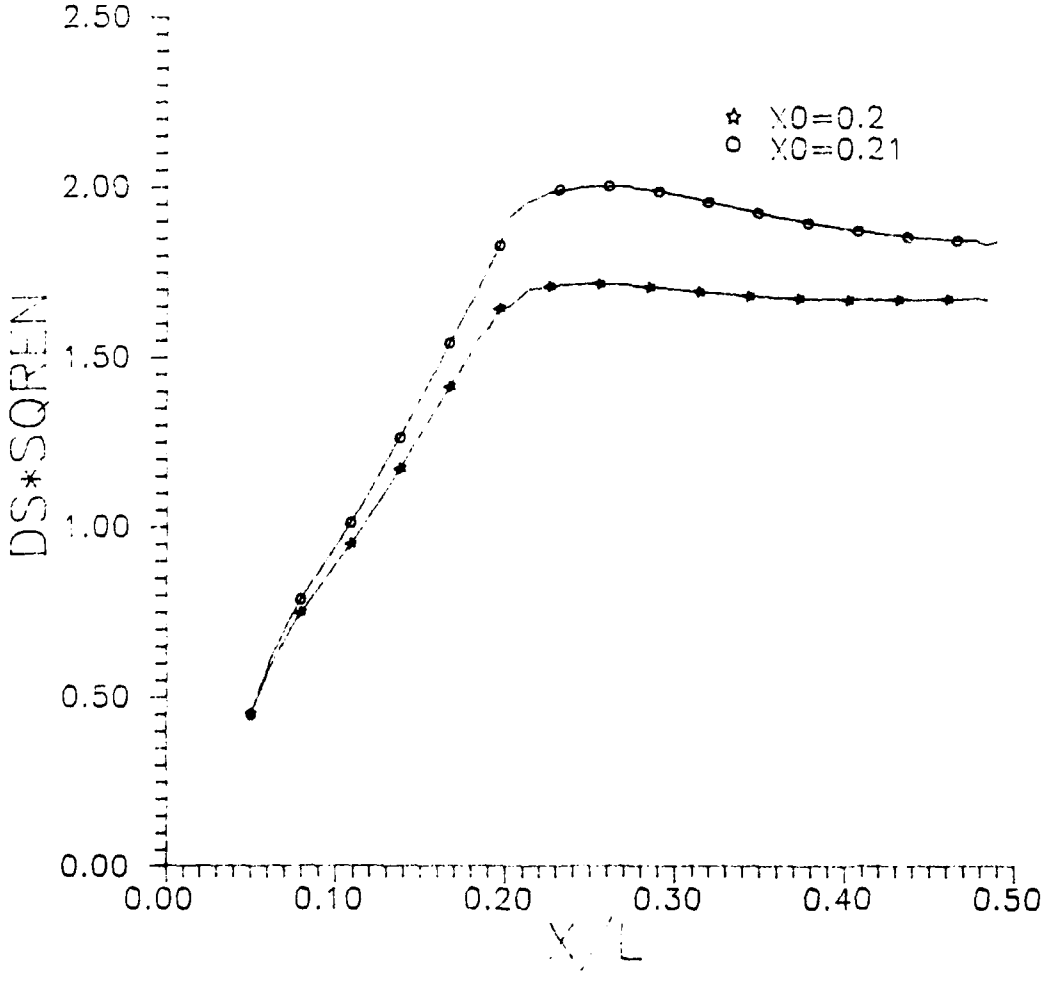

Figure 20. Displacement thickness for Method III

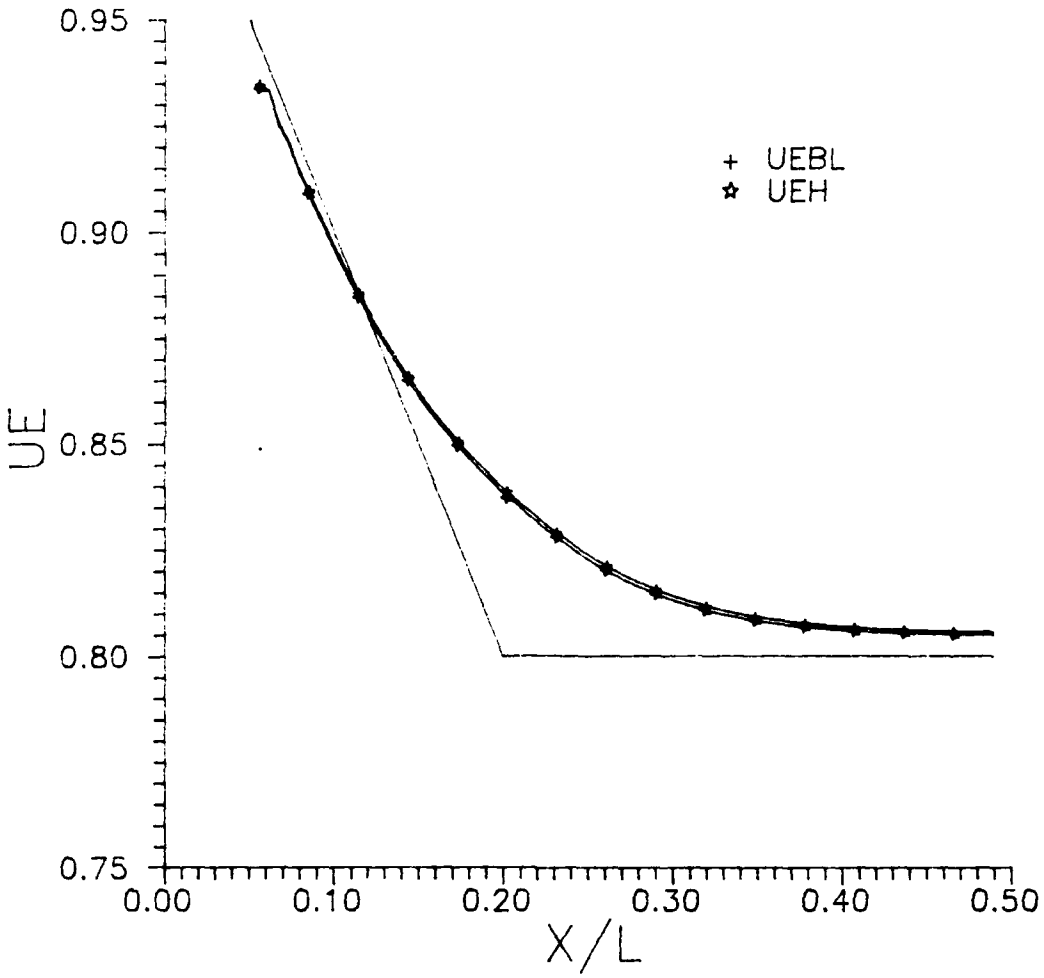

Figure 21. Edge velocities for Method III

The CPU time for this method was 60 seconds. An over-relaxation of the solution was used where W=1.3. The convergence criteria specified that the maximum difference between UEBL and UEH at any x location be less than 15×10^{-4}. This criteria resulted in 39 iterations to achieve convergence. The convergence history is shown in Figure 22. The ordinate represents the error in U_e normalized from the error of the first iteration. The method required approximately 14900 words of memory.

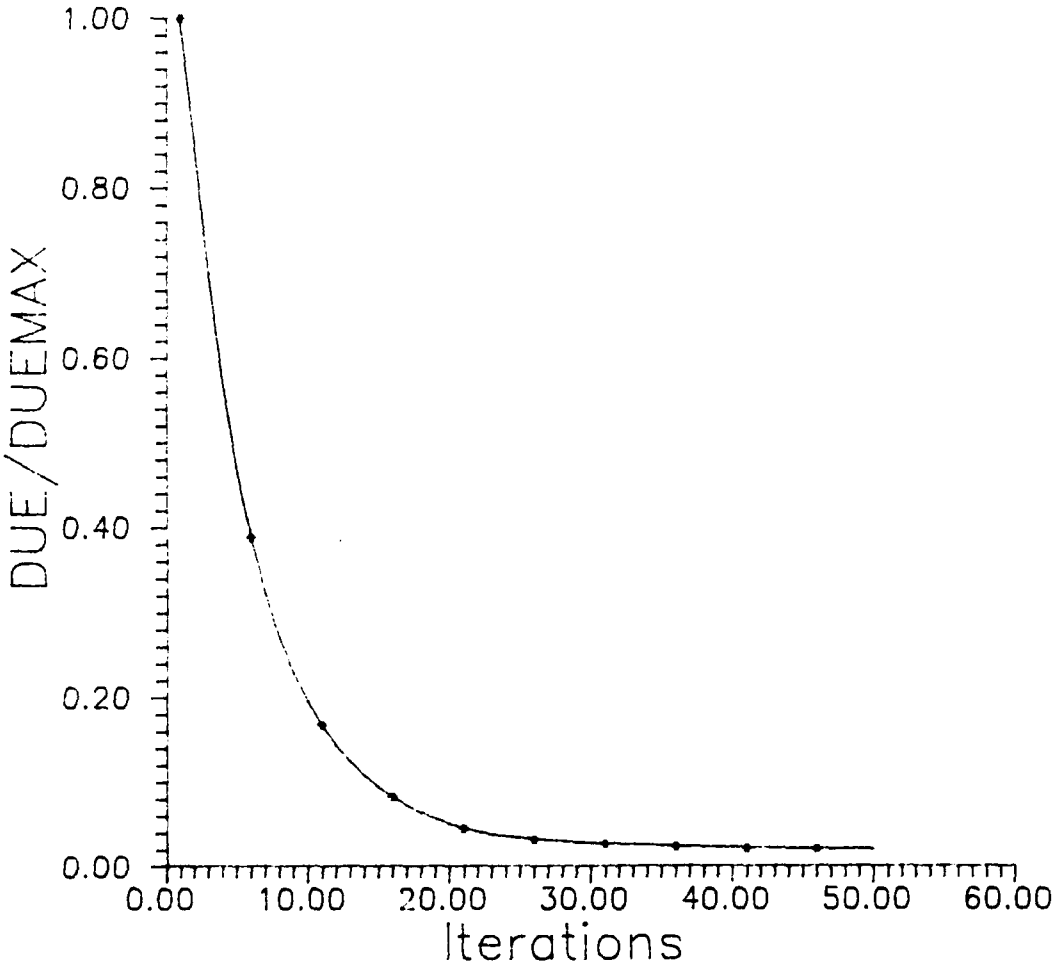

Figure 22. Convergence history for Method III

Comparison of Results

The CPU times and memory requirements are summarized in Table 1. Also presented are the average absolute errors (taken over five points in x) between C_f of the current methods and Briley's C_f. For Method I, C_f from the intermediate grid is used in the comparison since the other methods have the same number of x points (See Figure 9). The skin friction coefficient for methods II and III can be found in Figures 15 and 19 respectively. In Figure 19, the $X_0 = 0.2$ case is used.

	CPU Time	Memory	Mean C_f error
Method I			
-course (30x35)	55 sec		
-inter. (76x74)	579 sec	14.6 KW	0.096
-fine (151x74)	4101 sec		
Method II (1 cycle)			
-viscous	0.122 sec		0.1
-inviscid (76x51)	38.500 sec	5.5* KW	
Method III	60 sec	14.9 KW	0.14**

Table 1. Summary data for Methods I,II, and III

* using local scheme to calculate residuals

** after smoothing

V Conclusions and Recommendations

Method I uses finite difference equations with SLOR sweeps for solving the ANS equations in the viscous region and the stream function equation in the inviscid region. An implicit coupling scheme matches the two solutions. The solutions obtained from Method I compared well with full Navier-Stokes solutions. The coupling scheme developed for this method provided an efficient means of patching the viscous and inviscid regions. In addition, an initial displacement thickness is not required to start the solution. The cycle time for the course grid was the fastest of any of the three methods, with the resulting skin friction coefficient very close to that of the finer grids.

Method II uses finite difference approximations for solving the stream function equation in the inviscid region and a fourth order Runge-Kutta method for solving the integral boundary layer equations in the viscous region. Method II was shown to give very good for the first iteration. Solutions for C_f past the first iteration become less accurate. It is recommended that a velocity profile specified by a higher order polynomial be used to determine if an improvement in the stability of the solution can be achieved. The major contribution of this method is the efficient viscous solver. The solution to the boundary layer equations was reduced to finding the solution to a coupled

set of first order, ordinary differential equations that were solved using a simple fourth order Runge-Kutta method.

Method III obtained the inviscid flow solution by a panel method, while the viscous flow solution is obtained using the finite difference form of the boundary layer equations operating in an inverse scheme. The solutions obtained from Method III were in general agreement with the known solutions.

For the current model problem and geometry, Method I provided the best overall performance as evidenced by the data given in Table 1 of Chapter 4. However, for more complex geometries, Method II would have the best potential for providing efficient solutions with a minimal amount of required memory.

Any further study of these methods should consider the extension to 3-D flow, compressible flow, and also to flow over more realistic geometries.

Appendix A: Tridiagonal System Solvers

Single System of Equations

This algorithm was obtained directly from Appendix A of Reference [1]. It is used in the current work to solve the system of equations resulting from the finite difference form of Laplace's equation, written in general form as

$$A_j \Psi_{i,j-1} + B_j \Psi_{i,j} + C_j \Psi_{i,j+1} = RHS_j \qquad (a1)$$

where i is fixed and j varies from j=2 near the interface to j=JM1 near the outer boundary. Writing Eqn (a1) for all values of j results in the matrix equation

$$\begin{bmatrix} B_{i,2} & C_{i,2} & \cdots & 0 \\ A_{i,3} & B_{i,3} & \cdots & C_{i,3} \\ \vdots & & & \\ 0 & A_{i,JM1} & & C_{i,JM1} \end{bmatrix} \begin{bmatrix} \Psi_{i,2} \\ \Psi_{i,3} \\ \vdots \\ \Psi_{i,JM1} \end{bmatrix} = \begin{bmatrix} RHS_2 \\ RHS_3 \\ \vdots \\ RHS_{JM1} \end{bmatrix} \qquad (a2)$$

where the terms $A_{i,2}$ and $C_{i,JM1}$ are written in terms of the remaining coefficients from the boundary conditions. The algorithm simply takes matrix (a2) and cast it into upper triangular form by performing a series of row operations, given as

$$B_{i,j} = B_{i,j} - A_{i,j} C_{i,j-1} / B_{i,j-1} \qquad (a3)$$

$$RHS_j = RHS_j - A_{i,j} RHS_{i,j-1} / B_{i,j-1} \qquad (a4)$$

Where the equal sign implies replacement as in the FORTRAN programming language. The upper diagonal terms remain unchanged because of the tridiagonal form of the equations. The equations can now be solved by simple back substitution starting at j=JM1 and marching upwards.

Block Tridiagonal Solver

This algorithm was obtained from Reference [22]. The general features of the solver are exactly like that of the Thomas algorithm described in [1] except for the current case a block 2x2 set of equations exist.

The finite difference representations of the governing equations can be written in the following general form

$$A_1 \Psi_{J-1} + B_1 \Psi_J + C_1 \Psi_{J+1} + D_1 \omega_{J-1} + E_1 \omega_J + F_1 \omega_{J-1} = G_1 \quad (a5)$$

$$A_2 \Psi_{J-1} + B_2 \Psi_J + C_2 \Psi_{J+1} + D_2 \omega_{J-1} + E_2 \omega_J + F_2 \omega_{J-1} = G_2 \quad (a6)$$

where the coefficients are functions of the grid and the J subscripts denote the normal direction. Define the recurrence relations as

$$\Psi_J = R_{1J} \Psi_{J+1} + S_{1J} \omega_{J+1} + T_{1J} \quad (a7)$$

$$W_J = R_{2J} \Psi_{J+1} + S_{2J} \omega_{J+1} + T_{2J} \quad (a8)$$

Equations (a3) and (a4) were chosen this way to allow for a marching scheme that calculated the recurrence coefficients $R_1, S_1, T_1, R_2, S_2, T_2$ starting at J=0 and marching towards J=JMAX. Then the solution Ψ_J, ω_J are found by knowing the boundary condition at JMAX and marching the solution towards J=0 knowing the recurrence coefficients. The marching direction is arbitrary, but choosing the marching in this way is compatible with the development of the viscous/inviscid coupling scheme used in the present work.

Substitute (a7) and (a8) into (a5) and (a6) to get

$$A_1(R_{1,J-1}\,\Psi_J + S_{1,J-1}\,\omega_J + T_{1,J-1}) + B_1\,\Psi_J + C_1\,\Psi_{J+1} + D_1(R_{2,J-1}\Psi_J + S_{2,J-1}\,\omega_J + T_{2,J-1}) + E_1\,\omega_J + F_1\,\omega_{J+1} = G_1 \qquad (a9)$$

and

$$A_2(R_{1,J-1}\,\Psi_J + S_{1,J-1}\,\omega_J + T_{1,J-1}) + B_2\,\Psi_J + C_2\,\Psi_{J-1} + D_2(R_{2,J-1}\Psi_J + S_{2,J-1}\,\omega_J + T_{2,J-1}) + E_2\,\omega_J + F_2\,\omega_{J+1} = G_2 \qquad (a10)$$

Now rearrange (a9) and (a10) into the form

$$a_1\,\Psi_J + C_1\,\Psi_{J+1} + b_1\,\omega_J + F_1\,\omega_{J+1} = d_1 \qquad (a11)$$

$$a_2\,\Psi_J + C_2\,\Psi_{J+1} + b_2\,\omega_J + F_2\,\omega_{J+1} = d_2 \qquad (a12)$$

where

$$a_1 = B_1 + A_1\,R_{1,J-1} + D_1\,R_{2,J-1} \qquad (a13)$$

$$a_2 = B_2 + A_2\,R_{1,J-1} + D_2\,R_{2,J-1} \qquad (a14)$$

$$b_1 = E_1 + A_1\,S_{1,J-1} + D_1\,S_{2,J-1} \qquad (a15)$$

$$b_2 = E_2 + A_2\,S_{1,J-1} + D_2\,S_{2,J-1} \qquad (a16)$$

$$d_1 = G_1 - A_1\,T_{1,J-1} - D_1\,T_{2,J-1} \qquad (a17)$$

$$d_2 = G_2 - A_2\,T_{1,J-1} - D_2\,T_{2,J-1} \qquad (a18)$$

Now multiply Eqn (a11) by b_2 and multiply Eqn (a12) by b_1 and subtract. The resulting equation after some rearranging is

$$\Psi_J = ((C_2\,b_1 - C_1\,b_2)/D_0)\,\Psi_{J+1} + ((F_2\,b_1 - F_1\,b_2)/D_0)\,\omega_{J+1} + ((d_1\,b_2 - d_2\,b_1)/D_0) \qquad (a19)$$

where

$$D_0 = a_1\,b_2 - a_2\,b_1 \qquad (a20)$$

Compare Eqn (a19) to Eqn (a7) to find

$$R_{1J} = (C_2\ b_1 - C_1\ b_2)/D_0 \qquad (a21)$$

$$S_{1J} = (F_2\ b_1 - F_1\ b_2)/D_0 \qquad (a22)$$

$$T_{1J} = (d_1\ b_2 - d_2\ b_1)/D_0 \qquad (a23)$$

The remaining recurrence coefficients are found by multiplying Eqn (a11) by a_2 and multiplying Eqn (a12) by a_1 and subtracting. The vorticity is rearranged in the form of Eqn (a8) to find the recurrence

$$R_{2J} = (C_1\ a_2 - C_2\ a_1)/D_0 \qquad (a24)$$

$$S_{2J} = (F_1\ a_2 - F_2\ a_1)/D_0 \qquad (a25)$$

$$T_{2J} = (a_1\ d_2 - a_2\ d_1)/D_0 \qquad (a26)$$

With the recurrence known, the solution can be obtained from Eqns (a7) and (a8). Notice from Eqns (a13)- (a18) that the recurrence at the J-1 level are needed to generate the solution. The specification of the boundary conditions at the wall (J=1) gives the recurrence for J=1. Knowing this, the remaining recurrence are calculated.

Appendix B: Finite Difference Expressions

The general finite difference expressions for the derivatives in the governing equations are presented here. Because of the marching scheme, the derivatives in the normal (y) direction can be taken as central difference while the streamwise derivatives are generally taken as either forward or backward difference depending on the flow direction. The elliptic Ψ_{xx} term is taken as central difference.

A non-uniform grid is assumed where the coordinates (x,y) represent the physical domain and (ξ,η) represent the computational domain with indices i,j respectively. The metrics of the transformation are calculated as

$$\eta_{y|j} = 0.5 \left(\eta_{y|j+1/2} + \eta_{y|j-1/2} \right) \tag{b1}$$

where,

$$\eta_{y|j+1/2} = \Delta\eta/(y_{j+1} - y_j) \tag{b2}$$

$$\eta_{y|j-1/2} = \Delta\eta/(y_j - y_{j-1}) \tag{b3}$$

and

$$\xi_{x|i} = 0.5 \left(\xi_{x|i+1/2} + \xi_{x|i-1/2} \right) \tag{b4}$$

where,

$$\xi_{x|i+1/2} = \Delta\xi/(x_{i+1} - x_i) \tag{b5}$$

$$\xi_{x|i-1/2} = \Delta\xi/(x_i - x_{i-1}) \tag{b6}$$

The derivatives calculated in the physical domain can now be expressed in terms of the computational domain by simple application of the chain rule.

$$\psi_{y|j} = 0.5 \left(\psi_{y|j+1/2} + \psi_{y|j-1/2} \right)$$

$$= 0.5 \left(\eta_{y|j+1/2} \psi_{\eta|j+1/2} + \eta_{y|j-1/2} \psi_{\eta|j-1/2} \right)$$

$$= 0.5 \eta_{y|j+1/2} \left(\psi_{j+1} - \psi_j \right) / \Delta\eta$$

$$+ 0.5 \eta_{y|j-1/2} \left(\psi_j - \psi_{j-1} \right) / \Delta\eta$$

$$= 0.5/\Delta\eta \left[\eta_{y|j+1/2} \psi_{j+1} - \left(\eta_{y|j+1/2} - \eta_{y|j-1/2} \right) \psi_j \right.$$

$$\left. - \eta_{y|j-1/2} \psi_{j-1} \right]$$

$$= P_{1j} \psi_{j+1} + P_{2j} \psi_j - P_{3j} \psi_{j-1} \qquad \text{(b7)}$$

where,

$$P_{1j} = 0.5 \eta_{y|j+1/2} / \Delta\eta \qquad \text{(b8)}$$

$$P_{2j} = -0.5 \left(\eta_{y|j+1/2} - \eta_{y|j-1/2} \right) / \Delta\eta \qquad \text{(b9)}$$

$$P_{3j} = 0.5 \eta_{y|j-1/2} / \Delta\eta \qquad \text{(b10)}$$

Similarly,

$$\omega_{y|j} = P_{1j} \omega_{j+1} + P_{2j} \omega_j - P_{3j} \omega_{j-1} \qquad \text{(b11)}$$

The first derivative expressions in x are simply

$$\psi_{x|i} = \xi_{x|i} \left(\psi_i - \psi_{i-1} \right) / \Delta\xi \qquad \text{(b12)}$$

$$\omega_{x|i} = \xi_{x|i} \left(\omega_i - \omega_{i-1} \right) / \Delta\xi \qquad \text{(b13)}$$

The second derivatives are found as follows

$$\psi_{yy|j} = \eta_{y|j}\, \partial/\partial\eta(\psi_y)$$

$$= \eta_{y|j} \left(\psi_{y|j+1/2} - \psi_{y|j-1/2} \right) / \Delta\eta$$

$$= \eta_{y|j} (\eta_{y|j+1/2}\, \psi_{\eta|j+1/2} - \eta_{y|j-1/2}\, \psi_{\eta|j-1/2}) / \Delta\eta$$

$$= Q_{1j}\, \psi_{j+1} - Q_{2j}\, \psi_j + Q_{3j}\, \psi_{j-1} \qquad (b14)$$

where,

$$Q_{1j} = \eta_{y|j}\, \eta_{y|j+1/2} / \Delta\eta^2 \qquad (b15)$$

$$Q_{2j} = \eta_{y|j} \left(\eta_{y|j+1/2} + \eta_{y|j-1/2} \right) / \Delta\eta^2 \qquad (b16)$$

$$Q_{3j} = \eta_{y|j}\, \eta_{y|j-1/2} / \Delta\eta^2 \qquad (b17)$$

Similarly,

$$\omega_{yy|j} = Q_{1j}\, \omega_{j+1} - Q_{2j}\, \omega_j + Q_{3j}\, \omega_{j-1} \qquad (b18)$$

The second derivatives in x will have the same form as the y derivatives with the metrics interchanged, therefore

$$\psi_{xx|i} = K_{1i}\, \psi_{i+1} - K_{2i}\, \psi_i + K_{3i}\, \psi_{i-1} \qquad (b19)$$

where,

$$K_{1i} = \xi_{x|i}\, \xi_{x|i+1/2} / \Delta\xi^2 \qquad (b20)$$

$$K_{2i} = \xi_{x|i} \left(\xi_{x|i+1/2} + \xi_{x|i-1/2} \right) / \Delta\xi^2 \qquad (b21)$$

$$K_{3i} = \xi_{x|i}\, \xi_{x|i-1/2} / \Delta\xi^2 \qquad (b22)$$

Appendix C: Details of Method II

The calculation of δ^* and θ in Eqns (3.92) and (3.95) will be shown here in greater detail. The development of the functions $F_1(C_f,\delta)$ and $F_2(C_f,\delta)$ are also presented. Method II assumes a velocity profile given by Eqn (3.88) with the non-dimensional coefficients given in Eqn (3.91). Substituting (3.88) into Eqn (2.32), repeated here as

$$\delta^* = \int_0^\delta (1-u/U_e)\, dy \qquad (c1)$$

yields

$$\delta^* = \int_0^\delta \Big[\, 1 - 0.5R_eC_fU_e^{-1}y - ((10/3)\delta^{-2} - R_eC_f\delta^{-1}U_e^{-1})y^2 - (R_eC_fU_e^{-1}\delta^{-3} - 5\delta^{-4})y^4 - ((8/3)\delta^{-5} - 0.5R_eC_fU_e^{-1}\delta^{-4})y^5\Big] \qquad (c2)$$

Integrating Eqn (c2) gives

$$\delta^* = y - 0.25R_eC_fU_e^{-1}y^2 - (1/3)\Big[(10/3)\delta^{-2} - R_eC_f\delta^{-1}U_e^{-1}\Big]y^3 - (1/5)\Big[R_eC_fU_e^{-1}\delta^{-3} - 5\delta^{-4}\Big]y^5 - (1/6)\Big[(8/3)\delta^{-5} - 0.5R_eC_fU_e^{-1}\delta^{-4}\Big]y^6 \Big|_0^\delta \qquad (c3)$$

which results in

$$\delta^* = \delta - 0.25R_eC_fU_e^{-1}\delta^2 - (10/9)\delta + (1/3)R_eC_fU_e^{-1}\delta^2 - (1/5)R_eC_fU_e^{-1}\delta^2 + \delta - (4/9)\delta + (1/12)R_eC_fU_e^{-1}\delta^2 \qquad (c4)$$

Eqn (c4) simplifies to

$$\delta^* = (4/9)\delta - (1/30)R_e\, C_fU_e^{-1}\delta^2 \qquad (c5)$$

which is Eqn (3.92) with the terms A and B from Eqns (3.93) and (3.94) respectively.

To obtain the expression for θ in Eqn (3.95), substitute the velocity profile, Eqn (3.88), into Eqn (2.33), repeated here as

$$\theta = \int_0^{\delta} \left[(u/U_e) - (u/U_e)^2\right] dy \qquad (c6)$$

where the velocity profile can be written as

$$u = BU\, y + CU\, y^2 + EU\, y^4 + FU\, y^5 \qquad (c7)$$

when BU, CU, EU, and FU are given by Eqn (3.91). Squaring Eqn (c7) results in

$$u^2 = BU^2y^2 + 2(BU)CUy^3 + 2(BU)EUy^5 + 2((BU)FU+(CU)EU)y^6 + CU^2y^4 + 2(CU)FUy^7 + EU^2y^8 + 2(EU)FUy^9 + FU^2y^{10} \qquad (c8)$$

Substituting Eqns (c7) and (c8) into Eqn (c6) results in

$$\theta = \int_0^{\delta} \Big[(BU)U_e^{-1}y + (CU)U_e^{-1}y^2 + (EU)U_e^{-1}y^4 + (FU)U_e^{-1}y^5 - (BU)^2U_e^{-2}y^2 - 2BU(CU)U_e^{-2}y^3 - 2BU(EU)U_e^{-2}y^5 - 2(BU(FU)+(CU)EU)U_e^{-2}y^6 - (CU)^2U_e^{-2}y^4 - 2CU(FU)U_e^{-2}y^7 - (EU)^2U_e^{-2}y^8 - 2FU(EU)U_e^{-2}y^9 - (FU)^2U_e^{-2}y^{10}\Big]\, dy \qquad (c9)$$

where,

$$(BU)^2 = R_e^2C_f^2/4 \qquad (c10)$$

$$BU(CU) = (5/3)R_eC_fU_e\delta^{-2} - (1/2)R_e^2C_f^2\delta^{-1} \qquad (c11)$$

$$BU(EU) = (1/2)R_e^2C_f^2\delta^{-3} - (5/2)R_eC_fU_e\delta^{-4} \qquad (c12)$$

$$BU(FU) = (4/3)R_eC_fU_e\delta^{-5} - (1/4)R_e^2C_f^2\delta^{-4} \qquad (c13)$$

$$CU(EU) = (25/3)R_eC_fU_e\delta^{-5} - R_e^2C_f^2\delta^{-4} - (50/3)U_e^2\delta^{-6} \qquad (c14)$$

$$BU(FU)+CU(EU) = (29/3)R_e C_f U_e \delta^{-5} - (5/4)R_e{}^2 C_f{}^2 \delta^{-4} - (50/3)U_e{}^2 \delta^{-6} \quad (c15)$$

$$(CU)^2 = (100/9)U_e{}^2 \delta^{-4} - (20/3)R_e C_f U_e \delta^{-3} - R_e{}^2 C_f{}^2 \delta^{-2} \quad (c16)$$

$$CU(FU) = (80/9)U_e{}^2 \delta^{-7} - (13/3)R_e C_f U_e \delta^{-6} + (1/2)R_e{}^2 C_f{}^2 \delta^{-5} \quad (c17)$$

$$(EU)^2 = R_e{}^2 C_f{}^2 \delta^{-6} - 10 R_e C_f U_e \delta^{-7} + 25 U_e{}^2 \delta^{-8} \quad (c18)$$

$$EU(FU) = (31/6)R_e C_f U_e \delta^{-8} - (40/3)U_e{}^2 \delta^{-9} - (1/2)R_e{}^2 C_f{}^2 \delta^{-7} \quad (c19)$$

$$(FU)^2 = (64/9)U_e{}^2 \delta^{-10} - (8/3)R_e C_f U_e \delta^{-9} + (1/4)R_e{}^2 C_f{}^2 \delta^{-8} \quad (c20)$$

Now integrate Eqn (c9) and substitute in Eqns (c10)-(c20) to obtain

$$\theta = (1/4)\, R_e C_f \delta^2 U_e^{-1} + (1/3)U_e^{-1}\left[(10/3)U_e\delta^{-2} - R_e C_f \delta^{-1}\right]\delta^3$$
$$+ (1/5)U_e^{-1}\left[R_e C_f \delta^{-3} - 5U_e\delta^{-4}\right]\delta^5$$
$$+ (1/6)U_e^{-1}\left[(8/3)U_e\delta^{-5} - (1/2)R_e C_f \delta^{-4}\right]\delta^6$$
$$- (1/3)U_e^{-2}\left[R_e^2 C_f^2/4\right]\delta^3$$
$$- (1/2)U_e^{-2}\left[(5/3)R_e C_f U_e\delta^{-2} - (1/2)R_e^2 C_f^2\delta^{-1}\right]\delta^4$$
$$- (1/3)U_e^{-2}\left[(1/2)R_e^2 C_f^2\delta^{-3} - (5/2)R_e C_f U_e\delta^{-4}\right]\delta^6$$
$$- (2/7)U_e^{-2}\left[(29/3)R_e C_f U_e\delta^{-5} - (5/4)R_e^2 C_f^2\delta^{-4} - (50/3)U_e^2\delta^{-6}\right]\delta^7$$
$$- (1/5)U_e^{-2}\left[(100/9)U_e^2\delta^{-4} - (20/3)R_e C_f U_e\delta^{-3} + R_e^2 C_f^2\delta^{-2}\right]\delta^5$$
$$- (1/4)U_e^{-2}\left[(80/9)U_e^2\delta^{-7} - (13/3)R_e C_f U_e\delta^{-6} + (1/2)R_e^2 C_f^2\delta^{-5}\right]\delta^8$$
$$- (1/9)U_e^{-2}\left[R_e^2 C_f^2\delta^{-6} - 10R_e C_f U_e\delta^{-7} + 25U_e^2\delta^{-8}\right]\delta^9$$
$$- (1/5)U_e^{-2}\left[(31/6)R_e C_f U_e\delta^{-8} - (40/3)U_e^2\delta^{-9} - (1/2)R_e^2 C_f^2\delta^{-7}\right]\delta^{10}$$
$$-(1/11)U_e^{-2}\left[(64/9)U_e^2\delta^{-10} - (8/3)R_e C_f U_e\delta^{-9} + (1/4)R_e^2 C_f^2\delta^{-8}\right]\delta^{11} \qquad (c21)$$

Collect common terms in Eqn (c21) to obtain

$$\theta = \left[(10/9) - 1 + (4/9) + (100/21) - (100/45) - (80/36) - (25/9)\right.$$
$$\left. + (8/3) - (64/99)\right]\delta + \left[(1/4) - (1/3) + (1/5) - (1/12) - (5/6) + (5/6)\right.$$
$$\left. - (58/21) + (4/3) + (13/12) + (10/9) - (31/30) + (8/33)\right]R_e C_f \delta^2 U_e^{-1}$$
$$+\left[(-1/12) + (1/4) - (1/6) + (10/28) - (1/5) - (1/8) - (1/9) + (1/10)\right.$$
$$\left. - (1/44)\right]R_e^2 C_f^2 \delta^3 U_e^{-2} \qquad (c22)$$

Eqn (c22) reduces to

$$\theta \cong 0.1154401155\delta + 8.297258e\text{-}03\ R_e C_f \delta^2 U_e^{-1}$$
$$-1.695526e\text{-}03\ R_e^2 C_f^2 \delta^3 U_e^{-2} \qquad (c23)$$

which is simply Eqn (3.95) with the values of C,D, and E given by Eqns (3.96)-(3.98) respectively.

The expressions for $F_1(C_f,\delta)$ and $F_2(C_f,\delta)$ will now be derived. The process starts be writing Eqns (2.37) and (2.39) in terms of C_f and δ. This results in Eqns (3.101) and (3.102), repeated here as

$$2U_e U_{ex} C\delta + CU_e^2\delta_x + DU_{ex} C_f \delta^2 + DU_e \delta^2 C_{fx} + 2DU_e C_f \delta\delta_x$$
$$-2EC_f\delta^3 C_{fx} - 3EC_f^2\delta^2\delta_x - U_e^2 C_f/2 + U_e U_{ex} A\delta$$
$$- BU_{ex} C_f \delta^2 = 0 \qquad (3.101)$$

and

$$V_e = A\delta_x U_e + A\delta U_{ex} - 2BC_f\delta\delta_x - B\delta^2 C_{fx} - U_{ex}\delta \qquad (3.102)$$

To find $F_1(C_f,\delta)$, solve for C_{fx} in Eqn (3.101) and substitute into Eqn (3.102). The first step results in

$$C_{fx} = \Big[-CU_e^2\delta_x - 2C\delta U_e U_{ex} - DC_f\delta^2 U_{ex} - 2DC_f\delta\delta_x U_e$$
$$+3EC_f^2\delta^2\delta_x + (1/2)C_f U_e^2 - U_e U_{ex} A\delta + BU_{ex} C_f \delta^2 \Big]/z \qquad (c24)$$

where,

$$z = DU_e\delta^2 - 2EC_f\delta^3 \qquad (c25)$$

Substituting Eqn (c24) into (3.102) results in

$$V_e = A\delta_x U_e + A\delta U_{ex} - 2BC_f\delta\delta_x$$
$$-B\delta^2\left[-CU_e{}^2\delta_x z^{-1} - 2C\delta U_e U_{ex} z^{-1} - DC_f\delta^2 U_{ex} z^{-1} - 2DC_f\delta\delta_x U_e z^{-1}\right.$$
$$\left.+3EC_f{}^2\delta^2\delta_x z^{-1}+(1/2)C_f U_e{}^2 z^{-1}-U_e U_{ex} A\delta z^{-1}+BU_{ex}C_f\delta^2 z^{-1}\right]-U_{ex}\delta \qquad (c26)$$

The term δ_x can now be solved in terms of C_f and δ from Eqn (c.26), yielding

$$\delta_x = \left[-A\delta U_{ex} - 2BC\delta^3 U_e z^{-1} U_{ex} - BDC_f\delta^4 z^{-1} U_{ex} + (1/2)BC_f\delta^2 U_e{}^2 z^{-1}\right.$$
$$\left.-BU_e A\delta^3 z^{-1} U_{ex} + B^2 C_f\delta^4 z^{-1} U_{ex} + U_{ex}\delta + V_e\right]/K \qquad (c27)$$

where,

$$K = AU_e - 2BC_f\delta + BC\delta^2 U_e{}^2 z^{-1} + 2BDC_f\delta^3 U_e z^{-1} - 3BEC_f{}^2\delta^4 z^{-1} \qquad (c28)$$

Eqn (c27) is Eqn (3.103) of Chapter 3, where δ_x equals $F_1(C_f,\delta)$ from Eqn (3.99). $F_2(C_f,\delta)$ is found by solving for δ_x in Eqn (3.102) and substituting into Eqn (3.101). The first step results in

$$\delta_x = \left[V_e - A\delta U_{ex} + \delta U_{ex} + B\delta^2 C_{fx}\right]/P \qquad (c29)$$

where,

$$P = A\,U_e - 2B\,C_f\delta \qquad (c30)$$

Eqn (c29) can be simplified further by grouping the terms that do not contain C_{fx}, that is

$$\delta_x = Q + B\delta^2 C_{fx} P^{-1} \qquad (c31)$$

where,

$$Q = \left[V_e - A\delta U_{ex} + \delta U_{ex}\right]/P \qquad (c32)$$

Now substitute Eqn (c31) into Eqn (3.101) to obtain

$$2C\delta U_e U_{ex} + CU_e^2\left[Q + B\delta^2 C_{fx} P^{-1}\right] + DU_{ex} C_f \delta^2 + DU_e \delta^2 C_{fx}$$
$$+2DU_e C_f \delta\left[Q + B\delta^2 C_{fx} P^{-1}\right] - 2EC_f \delta^3 - 3EC_f^2 \delta^2\left[Q + B\delta^2 C_{fx} P^{-1}\right]$$
$$-(1/2)C_f U_e^2 + U_e U_{ex} A\delta - BU_{ex} C_f \delta^2 = 0 \qquad (c33)$$

Now solve for C_{fx} in Eqn (c33) to obtain

$$C_{fx} = \left[-2C\delta U_e U_{ex} - CU_e^2 Q - DU_{ex} C_f \delta^2 - 2DU_e C_f \delta Q + 3EC_f^2 \delta^2 Q \right.$$
$$\left. + (1/2)C_f U_e^2 - A\delta U_e U_{ex} + B\delta^2 C_f U_{ex}\right]/M \qquad (c34)$$

where,

$$M = BCU_e^2 \delta^2 P^{-1} + DU_e \delta^2 + 2BDU_e C_f \delta^3 P^{-1} - 2EC_f \delta^3 - 3BEC_f^2 \delta^4 P^{-1} \qquad (c35)$$

Eqn (c34) is Eqn (3.106) of Chapter 3, where C_{fx} equals $F_2(C_f, \delta)$ from Eqn (3.100).

Bibliography

1. Anderson, D.A., Tannehill, J.C., and Pletcher, R.H., Computational Fluid Mechanics and Heat Transfer. Hemisphere Publishing Corporation, New York, 1984.

2. Carter, J.E., "A New Boundary Layer Inviscid Iteration Technique for Separated Flow," AIAA Paper 78-1450, 1978.

3. Vatsa, V.N., Carter, J.E., and Swanson, R.C., "Comparison of Solutions of the Navier-Stokes and Interacting Boundary-Layer Equations for Separated Turbulent Flow," Proceedings of the ISCME International Conference on Computational Methods and Experimental Measurements, Washington, D.C., June 1982, pp. 283-295

4. Edwards, D.E. and Carter, J.E., "A quasi-Simultaneous Finite Difference Approach for Strongly Interacting Flow," Third Symposium on Numerical and Physical Aspects of Aerodynamic Flows, Long Beach, CA., Jan. 1985, pp. 163-174.

5. Houwink, R. and Veldman, A.E.P., "Steady and Unsteady Flow Computations for Transonic Airfoils," AIAA Paper 84-1618, 1984.

6. Rubin, S.G., Celestina, M., and Khosla, P.K., "Second Order Composite Velocity Solution for Large Reynolds Number Flows," AIAA Paper 84-172, 1984.

7. Swanson, R.C., Rubin, S.G., and Khosla, P.K., "Calculation of Afterbody Flows with a Composite Velocity Formulation." AIAA Paper 83-1736, 1983.

8. Halim, A. and Hafez, M., "Calculation of Separation Bubbles Using Boundary Layer-Type Equations," Recent Advances in Numerical Methods in Fluids, Vol. 3, Chap. 12, Pineridge Press, Swansea, United Kingdom, 1984, pp. 395-415.

9. Halim, A. and Hafez, M., "Calculation of Separation Bubbles Using Boundary Layer-Type Equations," AIAA Journal, Vol. 24, 1986, pp. 585-590.

10. Halim, A., "Development of an Iterative Boundary Layer-Type Solver for Axisymmetric Separated Flows," AIAA Journal, Vol. 24, Aug. 1986, pp. 1298-1304.

11. Halim, A., "Global Marching Technique for Predicting Separated Flows over Arbitrary Airfoils," AIAA Journal, Vol. 25, Sept. 1987, pp. 1263-1266.

12. Brown, S.N. and Stewartson, K., "Laminar Separation" Annual Review of Fluid Mechanics, William R. Sears and Milton Van Dyke, eds., Vol. 1, Annual Reviews, Inc., 1969, pp. 45-72.

13. Carter, J.E., "Inverse Solutions for Laminar Boundary Layer Flows with Separation and Reattachment," NASA TR R-447, 1975.

14. Meksyn, D., "New Methods in Laminar Boundary Layer Theory," Pergamon Press, Inc., 1961.

15. Howarth, L., "On the Solution of Laminar Boundary Layer Equations," Proc. Roy. Soc. (London), Ser. A, Vol. 164, No. 919, Feb. 1938, pp. 547-579.

16. Briley, W.R., "A Numerical Study of Laminar Separation Bubbles Using The Navier-Stokes Equations," J. of Fluid Mechanics, Vol. 47, June 1971, pp. 713-736.

17. Schlichting, H., Boundary Layer Theory, McGraw-Hill Book Company Inc., Fourth Edition, 1951.

18. Cebeci, T. and Bradshaw, P., Physical and Computational Aspects of Convective Heat Transfer, Springer-Verlag New York Inc., 1984.

19. White, F.M., Viscous Fluid Flow, McGraw-Hill Inc., 1974.

20. Chow, C.Y., An Introduction to Computational Fluid Mechanics, John Wiley and Sons, Inc., 1979.

21. Cebeci, T. and Stewartson, K., "On the calculation of separation bubbles," J. of Fluid Mechanics, Vol. 133, 1983, pp. 287-296

22. Werle, M.J. and Bernstein, J.M. "A Comparative Numerical Study of Approximations to the Navier-Stokes Equations for Incompressible Separated Flow," University of Cincinnati Report No. AFL 74-7-12, 1974.

VITA

Jeffrey C. Tromp [redacted] in 1978 [redacted] enrolled at Miami University of Oxford, Ohio the same year. After a year at Miami, he transferred to the University Of Cincinnati (UC) to pursue an engineering degree. In 1983, he graduated from UC with a Bachelors degree in Aerospace Engineering. He is currently employed at the Flight Dynamics Laboratory at Wright Patterson Air Force Base. In 1987, he was accepted into the Long-Term Full-Time Training program at the School of Engineering, Air Force Institute of Technology.

[redacted]

UNCLASSIFIED

SECURITY CLASSIFICATION OF THIS PAGE

REPORT DOCUMENTATION PAGE

Form Approved
OMB No. 0704-0188

1a. REPORT SECURITY CLASSIFICATION UNCLASSIFIED	1b. RESTRICTIVE MARKINGS
2a. SECURITY CLASSIFICATION AUTHORITY	3. DISTRIBUTION/AVAILABILITY OF REPORT Approved for public release; distribution unlimited
2b. DECLASSIFICATION/DOWNGRADING SCHEDULE	
4. PERFORMING ORGANIZATION REPORT NUMBER(S) AFIT/GA/AA/88S-1	5. MONITORING ORGANIZATION REPORT NUMBER(S)
6a. NAME OF PERFORMING ORGANIZATION School of Engineering 6b. OFFICE SYMBOL (If applicable) AFIT/ENY	7a. NAME OF MONITORING ORGANIZATION
6c. ADDRESS (City, State, and ZIP Code) Air Force Institute of Technology Wright Patterson AFB, OH 45433	7b. ADDRESS (City, State, and ZIP Code)
8a. NAME OF FUNDING/SPONSORING ORGANIZATION 8b. OFFICE SYMBOL (If applicable)	9. PROCUREMENT INSTRUMENT IDENTIFICATION NUMBER
8c. ADDRESS (City, State, and ZIP Code)	10. SOURCE OF FUNDING NUMBERS PROGRAM ELEMENT NO / PROJECT NO. / TASK NO / WORK UNIT ACCESSION NO.

11. TITLE (Include Security Classification)

NUMERICAL STUDY OF THREE VISCOUS/INVISCID INTERACTION METHODS (UNCLASSIFIED)

12. PERSONAL AUTHOR(S)
Jeffrey C. Tromp

13a. TYPE OF REPORT	13b. TIME COVERED	14. DATE OF REPORT (Year, Month, Day)	15. PAGE COUNT
MS Thesis	FROM _____ TO _____	1988, September	105

16. SUPPLEMENTARY NOTATION

17. COSATI CODES			18. SUBJECT TERMS (Continue on reverse if necessary and identify by block number)
FIELD	GROUP	SUB-GROUP	COMPUTATIONAL FLUID DYNAMICS, FLUID DYNAMICS, NAVIER-STOKES EQUATIONS
20	04		

19. ABSTRACT (Continue on reverse if necessary and identify by block number)

see reverse side

J. J. Paluniewicz
12 Jan 1989

20. DISTRIBUTION/AVAILABILITY OF ABSTRACT ☒ UNCLASSIFIED/UNLIMITED ☐ SAME AS RPT. ☐ DTIC USERS	21. ABSTRACT SECURITY CLASSIFICATION UNCLASSIFIED
22a. NAME OF RESPONSIBLE INDIVIDUAL Jeffrey C. Tromp	22b. TELEPHONE (Include Area Code) (513) 255-6526 22c. OFFICE SYMBOL AFWAL/FIGD

DD Form 1473, JUN 86 *Previous editions are obsolete.* SECURITY CLASSIFICATION OF THIS PAGE

UNCLASSIFIED

ABSTRACT

The study of flows with viscous/inviscid interaction has attracted many researchers over the last decade. These flows occur whenever the adverse pressure gradient is large enough to cause flow separation. The current emphasis is to find efficient ways of solving these types of flows without solving the full Navier-Stokes equations.

Three methods for solving the viscous/inviscid problem were studied. The first method uses finite difference equations to model both the viscous and inviscid regions. A coupling scheme is developed to match the two solutions. The second method solves the integral boundary layer equations in the viscous region and finite difference equations in the inviscid region. The third method solves the Hilbert integral to generate a correction to the inviscid velocity using the boundary layer equations as the viscous model. The model problem used in this work is Howarth flow over a flat plate.

The three methods were evaluated in terms of solution accuracy, memory requirements, and computation times.